C.P. No. 1376

C.P. No. 1376

PROCUREMENT EXECUTIVE, MINISTRY OF DEFENCE

AERONAUTICAL RESEARCH COUNCIL

CURRENT PAPERS

Numerical Methods for Two-Dimensional and Axisymmetric Transonic Flows

-by-

M. J. Langley

Aircraft Research Association Limited

LONDON: HER MAJESTY'S STATIONERY OFFICE

1977

£2.50 net

C.P. No.1376*
September 1973

NUMERICAL METHODS FOR TWO-DIMENSIONAL AND AXISYMMETRIC TRANSONIC FLOWS

- by -

M.J. Langley

SUMMARY

Two methods are presented for the calculation of transonic flows. Firstly a method is described for the design of aerofoils with prescribed pressure distributions including shock waves. The method is essentially an inversion of a numerically refined version of the Murman-Krupp technique for the solution of the transonic small perturbation equation with linearized boundary conditions. To demonstrate the usefulness and accuracy of the method examples are shown of the design of supercritical type aerofoil sections, the final results being compared with calculations by the nominally exact Garabedian & Korn analysis method.

The second method is for the calculation of axisymmetric transonic flow past bodies of revolution. Following Garabedian & Korn the exact potential flow equations are solved in the inside of the unit circle obtained from the body contour by conformal transformation. The particular problems of calculating axisymmetric flows by such methods are discussed and examples are shown of calculations by the present method compared with other methods and experimental data.

(Paper presented at Euromech 40, Stockholm, September 1973).

---

*Replaces A.R.C.34 701.

CONTENTS

CONTENTS (Continued)

FIGURES

1. INTRODUCTION

The most successful methods to date for the calculation of steady transonic flows have been finite difference techniques for the solution of either the small perturbation or the exact equations for the velocity potential. It was first shown by Murman and Cole[1] that by using difference schemes, retarded in the flow direction at all points in the hyperbolic region, solutions could be obtained for transonic flows in which the shock waves emerged in the course of the calculation. They presented solutions of the transonic small perturbation equation for the case of a sharp nosed non-lifting two dimensional aerofoil. Shortly afterwards the method was extended (Murman & Krupp[2,3]) to cover blunt nosed lifting aerofoils. The first method to be presented here is a development of the Murman-Cole-Krupp techniques for the design of aerofoils with prescribed pressure distributions including embedded shock waves. The two obvious alternatives to such a method are either laborious "cut and try" methods with alternate manual geometric modifications and forward calculation of the flow or the use of the hodograph methods of Nieuwland[4] or Korn[5]. The latter whilst awe-inspiring in the quality of the numerical analysis involved require a lot of experience to use and are valid for shock free flows only. Optimum aerofoils will usually, of course, not have shock free flows, weak shock waves being acceptable from both the wave drag and boundary layer separation viewpoints.

Solution of the transonic small perturbation equations with linearized boundary conditions produce surprisingly accurate solutions for many aerofoil shapes and provide a particularly convenient basis for design and three dimensional calculations. However the use of the exact inviscid potential equations is not only preferable but can, when allied with an efficient coordinate system provide simpler, faster solutions than the small perturbation techniques.

Thus the Bauer, Garabedian and Korn[5,6] and the similar Jameson[7]* methods are very important weapons in our armoury for the calculation of planar flows. The second method to be described is an extension of BGKJ methods to the calculation of the transonic flow about non-ducted axisymmetric bodies at zero incidence. For bluff nosed bodies of revolution the use of linearized boundary conditions is unlikely to give sufficient accuracy for practical purposes hence we have been forced to adopt the use of a Sells coordinate system for these calculations as in the BGKJ methods.

In section 2 the Murman-Krupp method is briefly described together with the improvements which we have made in order to increase its speed and accuracy. The design version is described and some examples of its use are given. Section 3 contains a description of the axisymmetric flow method and examples of calculations using it are shown.

2. TRANSONIC SMALL PERTURBATION DESIGN METHOD

2.1. Introduction

Although most people will be familiar with the Murman-Cole-Krupp method it will be convenient to describe it here in brief detail in order to bring out the differences between their basic method and the refined version we have developed at A.R.A. which has led to the design method.

The transonic small perturbation equation for the perturbation potential Φ

$$\left(1 - M_\infty^2 - (\gamma+1)\, M_\infty^2\, \frac{\partial \Phi}{\partial x}\right) \frac{\partial^2 \Phi}{\partial x^2} + \frac{\partial^2 \Phi}{\partial y^2} = 0$$

is rewritten as

$$\left(\frac{(1 - M_\infty^2)}{M_\infty^{2p}\, \delta^{2/3}} - (\gamma+1) M_\infty^{2-3p}\, \frac{\partial \phi}{\partial x}\right) \frac{\partial^2 \phi}{\partial x^2} + \frac{\partial^2 \phi}{\partial \tilde{y}^2} = 0$$

where $\tilde{y} = M_\infty^p\, \delta^{1/3}\, y, \quad \phi = M_\infty^p\, \delta^{-2/3}\, \Phi$

---

* Henceforth collectively called the BGKJ method.

and δ is the aerofoil thickness/chord ratio. The aerofoil shape being defined by $y = \delta Y_{u,\ell}(x)$, Fig.1, and p is an arbitrary power to be determined later.

The linearized boundary condition on the aerofoil

$$\frac{\partial \Phi}{\partial y}\ (x,\pm 0) \ = \ \delta Y'_{u,\ell}(x) - \alpha$$

then becomes

$$\frac{\partial \phi}{\partial \tilde{y}}\ (x,\pm 0) = Y'_{u,\ell}(x) - A, \quad A = \alpha/\delta$$

For M near 1 the equation can be further simplified to

$$\left(K - (\gamma+1)\ \frac{\partial \phi}{\partial x}\right)\ \frac{\partial^2 \phi}{\partial x^2} + \frac{\partial^2 \phi}{\partial \tilde{y}^2} \ = 0$$

where the transonic similarity parameter $K = \dfrac{1 - M_\infty^2}{M_\infty^{\,2p}\delta^{2/3}}$.

The perturbation velocity is strictly

$$u \ = \ \phi_x\, M_\infty^{-p}\delta^{2/3}$$

but Krupp allows himself the opportunity of writing

$$u \ = \ \phi_x M_\infty^{-q}\delta^{2/3} \quad , \quad q \neq p$$

and takes the first order equation

$$C_p \ = \ -2u$$

Krupp chose the two parameter p,q to obtain the best agreement with certain exact solutions and suggests the values $p = \frac{1}{2}$, $q = \frac{3}{4}$ should be used. Partly because our method is somewhat different to Krupp's we have found that taking p=0.425, and q=0.75 and then using the exact isentropic relationship

$$C_p \ = \frac{2}{1.4M_\infty^2} \quad \left\{\left[1 + 0.2\ M_\infty^2\ \left(1 - (1+u)^2\right)\right]^{3.5} - 1\right\}$$

gives superior results for the areas in which we have the most interest i.e. fairly thick lifting aerofoils. In particular shock wave position and the velocity level near the t.e. lower surface are more accurately predicted.

Krupp uses a non-equally spaced rectangular mesh in the $(x, \tilde{y})$ plane truncated some distance away from the aerofoil, the far field boundary condition being applied there using an approximation to the far field influence of a thin lifting aerofoil. In the main body of the flow field the Murman-Cole mixed finite difference scheme is used solving the equations along successive vertical lines, sweeping in the direction of the free stream flow. Both as regards the grid system and the finite difference scheme our version of the method is virtually identical* to the Murman-Krupp method. Where our method mainly differs to the original is in the treatment of circulation and the boundary conditions on the slit representing the aerofoil.

2.2. Treatment of Circulation

Krupp's far field approximation may be conveniently written

$$\phi(x,\tilde{y}) = \phi_{linear}(x,\tilde{y}) - \frac{\gamma_o}{2\pi} \arg\,(z + \sqrt{z^2 - 1})$$

$$z = x + i\,K^{\frac{1}{2}}\tilde{y}$$

The ϕ_{linear} term represents the contribution of the aerofoil thickness and camber which are known (for forward calculations) a priori. On the other hand the circulation γ_o is unknown and must be determined during the course of the calculations to satisfy the Kutta condition, which states that ϕ_x and ϕ_y must be continuous along the slit $\tilde{y}=0$, $x > 1$ downstream of the aerofoil trailing edge. Thus in a converged solution there is a jump in ϕ of value γ_o along $\tilde{y} = 0$, $x > 1$.

Krupp suggests an iterative scheme for the determination of γ_o in which the circulation at infinity (γ_{ff}) is periodically updated using an extrapolated value derived from the latest value of the jump in ϕ across the trailing edge and the value used at the last update. Differencing across the slit $x > 1$ is achieved by assuming a linear variation in the jump in ϕ between the trailing edge and the far field boundary. This technique is both cumbersome and slow to converge.

---

* the one exception to this is described in section 2.4 below.

Consider the following scheme. Referring to Fig.2 for the simplified case of a uniform mesh the difference approximations can be written

$$\phi_{\tilde{y}\tilde{y}|i,J^{\pm}} = \frac{1}{\Delta\tilde{y}} \left(\frac{\phi_{i,J+1} - \phi_{i,J+}}{\Delta\tilde{y}} - \frac{\phi_{i,J-} - \phi_{i,J-1}}{\Delta\tilde{y}} \right)$$

$$\phi_{xx|i,J^{\pm}} = \frac{1}{\Delta x^2} \left(\phi_{i+1,J^{\pm}} - 2\phi_{i,J^{\pm}} + \phi_{i-1,J^{\pm}} \right)$$

$$V_{i,J^{\pm}} = K - \frac{(\gamma+1)}{2\Delta x} \left(\phi_{i+1,J^{\pm}} - \phi_{i-1,J^{\pm}} \right)$$

where the continuity in ϕ_y has been implicitly assumed in the equation for $\phi_{\tilde{y}\tilde{y}}$.

The difference approximations to the small perturbation equation at (i,J+) and (i,J-) can then be written

$$V_{i,J^{\pm}} \quad \phi_{xx|i,J^{\pm}} + \phi_{\tilde{y}\tilde{y}|i,J^{\pm}} = 0$$

From the equation for (i,J-) $\phi_{i,J-}$ may be determined and substituted in the equation for (i,J+); this equation is then used in the finite difference scheme at column i, $\phi_{i,J-}$ being determined when required from the remaining equation.

Having removed any assumptions about the variation of the potential jump across the slit it is then possible to force the circulation in the field to change more rapidly. This is done by updating the circulation used in the far field boundary condition and the circulation in the main body of the flow field after every sweep through the field. This compares with only occasional updating of the far field boundary condition in the original Krupp method.

If $\Delta\phi_{te}$ is the change in the jump across the trailing edge between consecutive iterations then we increment ϕ in the far field by putting

$$\Delta\phi = \frac{\omega\Delta\phi_{te}}{2\pi} \arg\left(z + \sqrt{z^2-1}\right)$$

and in the rest of the field by

$$\Delta\phi = \frac{\omega\Delta\phi_{te}}{2\pi} \arg(z)$$

where ω is a relaxation factor (usually taken as 1.0).

This device is similar in principle to that used in the GKBJ methods but its application is more complicated in the small perturbation method and probably less effective. The amount of storage required is increased because of the need to store arg (z) at each mesh point but this disadvantage is usually outweighed by the decreased computation times.

2.3. Aerofoil boundary conditions

In Fig.3 the aerofoil boundary condition used by Krupp is shown diagrammatically. The difference equations are solved one mesh point above the slit by using

$$\phi_{\tilde{y}\tilde{y}|i,J+1} = \frac{2}{t(t+2s)}\left(\phi_{i,J+2} - \phi_{i,J+1}\right) - \frac{2}{t+2s}\,\phi_{\tilde{y}|i,J}$$

It is easily shown that the truncation error is minimised by using $s = t/\sqrt{3}$. Having obtained $\phi_{i,J+1}$ the values in the slit are obtained by linear extrapolation from the points (i,J+1) and (i,J+2).

It is important to maintain consistency between the boundary conditions used for the design and analysis methods. This is difficult using the Krupp scheme. It is preferable to solve for ϕ directly on the slit. This can be done quite simply by using

$$\phi_{\tilde{y}\tilde{y}|i,J} = \frac{2}{s^2}\left(\phi_{i,J+1} - \phi_{i,J} - s\phi_{\tilde{y}|i,J}\right)$$

The minimization of the truncation error in this case requires s to be small; in order to keep the truncation error to a minimum for the difference approximation to $\phi_{\tilde{y}\tilde{y}|i,J+1}$ it is necessary for s = t. It will be noted that the tridiagonal structure of the difference equations is maintained.

Figure 4 shows a comparison between pressure distributions obtained for a Korn aerofoil[8] using the two aerofoil boundary conditions. These calculations were done using the Krupp transonic similarity parameters and C_p definition. The differences are quite small.

2.4. Other alterations to the Murman-Krupp method

Two other significant changes have been made to the Krupp method, both of them tending to bring it into line with the BGKJ methods.

Firstly because of the non-linearity of the equations Krupp suggests iterative solution at each column until convergence is obtained. However this offers little improvement, in terms of the number of complete sweeps through the field required, compared with the use of just one iteration per column. An increase in speed by a factor of about 3 is obtained by this device.

The second major change is the introduction of mesh refinement. Three levels of mesh size are used employing 80x60, 40x30 and 20x15 mesh points, the larger number being in the stream direction. One sweep through the coarsest grid takes only one sixteenth of the time on the finest and, whilst of course, compared with the final solution the detailed pressure distributions at this level are poor, the general form is quite similar and the value of the circulation is fairly accurate.

2.5. Summary of improvements and examples

It is convenient at this point to summarise the changes we have made to the Murman-Krupp method in trying to improve its speed, accuracy and ease of conversion to a design mode.

(1) Optimised transonic similarity parameters and C_p definition,

(2) Treatment of circulation,

(3) Aerofoil boundary conditions,

(4) Column iteration removed,

(5) Mesh refinement.

Figures 5 and 6 show comparisons between the present method and more exact methods. The first figure shows computations for the Korn aerofoil[8] compared with results obtained by the BGK analysis and design methods[5]. The second example (fig.6) is for the NACA 0012 section at $M = 0.75$, $\alpha = 2^o$ also compared with results obtained using the Garabedian program. The agreement is good, the worst features being in the leading edge region on the upper surface, and near the trailing edge lower surface for the rear loaded section.

2.6. Design method - treatment of aerofoil boundary conditions

For aerofoil design the pressure coefficient C_p (and hence ϕ_x) is known over all or part of the aerofoil surface and it is required to determine the aerofoil shape which produces it.

The core of the design procedure is, of course, the treatment of the aerofoil boundary conditions. Various methods were tried before a satisfactory one was found. Initial attempts using modifications to the Krupp boundary conditions were unsuccessful because of the necessity to transfer information from the slit to one mesh point above. This led to the adoption of the aerofoil boundary conditions described in section 2.3 for forward calculations.

Methods which employ Dirichlet boundary conditions from

$$\phi = \int \phi_x dx$$

in which the integration is initiated near the leading edge of the aerofoil do not work because of the fixing of ϕ at the leading edge, this only being changed by information spreading from the aerofoil into the field and back again - a very slow process.

It was found that the only methods which converge quickly to satisfactorily accurate solutions are those in which successive forward calculations are made with regular updating of the aerofoil shapes to obtain the required ϕ_x distribution.

Two methods of updating the aerofoil shape and hence $\phi_{\tilde{y}}$ come to mind. We can either use the vorticity equation

$$\phi_{x\tilde{y}} = \phi_{\tilde{y}x} \quad , \quad \frac{\partial}{\partial x}(\phi_{\tilde{y}}) = \frac{\partial}{\partial \tilde{y}}(\phi_x)$$

or the governing partial differential equation

$$\left(K - (\gamma+1)\phi_x\right)\phi_{xx} + \phi_{\tilde{y}\tilde{y}} = 0$$

The values of ϕ_x (and ϕ_{xx}) can be calculated using the required surface values of ϕ_x. Solution of the equation then yields $\phi_{\tilde{y}}$.

Both equations have been tried and the one which has proved the most successful in terms of its convergence properties is the vorticity equation.

Briefly the scheme is as follows. The first few points on the aerofoil are specified, the method then being restricted to the modification of a known profile. For the remainder of the profile (either top, bottom or both surfaces) the pressure distribution ϕ_x is specified.

After each sweep though the field ϕ_{xy} is calculated on the aerofoil using

$$\phi^{n+\frac{1}{2}}_{x\tilde{y}|i,J} = \frac{1}{2s}\left(-3\phi^{n+\frac{1}{2}}_{x|i,J} + 4\phi^{n}_{x|i,J+1} - \phi^{n}_{x|i,J+2}\right)$$

$$\text{where} \quad \phi^{n+\frac{1}{2}}_{x|i,J} = \omega_1 \bar{\phi}_x + (1-\omega_1)\phi^{n}_{x|i,J}$$

ϕ^n_x is determined from central differences (even in the hyperbolic region) from the values of ϕ from the previous sweep. The superscript denotes iteration number and $\bar{\phi}_x$ is the required value of ϕ_x. The surface slopes

can then be calculated from $\phi^{n+\frac{1}{2}}_{\tilde{y}|i,J} = \int_{xo}^{xi} \phi^{n+\frac{1}{2}}_{x\tilde{y}|i,J}\, dx. + \phi_{\tilde{y}|x=xo}$

where x = xo is the last fixed point near the leading edge. The trapezium rule is sufficiently accurate for the integral. The values of the surface slopes used for the next sweep through the field are then

$$\phi^{n+1}_{\tilde{y}|i,J} = \omega_2\, \phi^{n+\frac{1}{2}}_{y|i,J} + (1-\omega_2)\phi^{n}_{y|i,J}$$

In order to obtain convergence the two relaxation parameters ω_1 and ω_2 have to be small, 0.1 and 0.3 being used.

This scheme is similar to that used by Steger and Klineberg[9] except that they used the perturbation velocity components as their main dependent variables.

2.7. Design method - far field boundary conditions etc.

The overall convergence of the method can be speeded up by rapidly changing the circulation over the whole field to that implied by the integration of the desired pressure distribution. The far field boundary condition, the transonic similarity factor and in fact the relationship between C_p and ϕ_x are all dependent on the aerofoil geometry. Thus all of these parameters have to be recalculated as part of an extra iteration sequence as the main calculation proceeds. In order to obtain convergence it is not possible to start these modifications until the major part of the aerofoil geometry modifications has been computed.

2.8. The design method in practice

It has been mentioned previously that the method is restricted to the modification of existing aerofoils. The restrictions imposed by this fact are not too severe. Rough designs for aerofoils are often available from previous designs or by use of one of the many approximate inverse subcritical methods. In addition the leading edge of an aerofoil is often optimised for

low or intermediate Mach number conditions where the performance is dominated by the leading edge velocity peak. It can thus be advantageous to optimise the high speed performance without disturbing the leading edge region.

To be fair, it would of course be an advantage to be able to specify the pressure distribution over the whole of the aerofoil surface.

Our computer program is arranged to have various design options. The upper surface and lower surface may be altered simultaneously or separately; alternatively the pressure distribution may be specified over the upper surface and the thickness distribution may be kept constant. This latter option is particularly useful as problems of crossed or too thick trailing edges may be avoided and having once found an aerofoil satisfying structural constraints, as far as the thickness distribution is concerned, this quality may be maintained.

Some expertise is needed of course in specifying the pressure distribution. In particular the pressure distribution away from the leading edge must be compatible with the fixed leading edge geometry. Changing the pressure distribution over the rear part of the aerofoil in general implies a changed circulation, this then alters the pressure distribution near the leading edge. After a major modification it is often useful to do a minor tidying-up operation to remove any unwanted blemishes in the pressure distribution. This will be demonstrated later.

Both in this case and in other conditions where the specified pressure distribution is not consistent with other features of the flow the program will usually converge to a smooth consistent result.

2.9. Run times

Taking a convergence criterion that $\max_{i,j} |\phi^{n}_{i,j} - \phi^{n-1}_{i,j}| < 5\times10^{-5}$ the number of iterations needed for forward calculations is usually about 200 - 300 on each of the coarser grids and between 100 - 250 on the fine (80 x 60) grid. 100 iterations on the finest grid would take about 45 secs.

on a CDC 6600. Design calculations can be completed in about 150-300 iterations on the fine grid.

2.10. Examples of use

The first example is of the successive modification of a NACA 0012 aerofoil to convert it into a shape having many of the characteristics of a supercritical aerofoil. This is shown in fig.7(a-d).

Starting with a forward calculation (fig.7(a)) we first specify a pressure distribution on the upper surface aft of 15% chord, shown by the dashed line. The shock wave has been weakened and moved rearwards by about 15% chord, and the upper surface rear loading has been increased. The lower surface shape is kept fixed. The pressure distribution output by the design program is shown by the dotted line. Note the new pressure distribution near the leading edge and the decreased velocities on the lower surface caused by the increased circulation.

The pressure distribution shown by the dotted line in Fig.7(a) becomes the starting solution in Fig.7(b). As mentioned previously a small tidy-up operation is now done near the leading edge. This is shown by the dashed and dotted lines.

Finally in Fig.7(c) lower surface rear loading is added by specifying a similar pressure distribution on the upper surface as in the previous figure, and the required lower surface pressure distribution (the dashed line). The aerofoil shape after this modification had too thick a trailing edge, this was thinned somewhat and the pressure distribution calculated. This is shown by the dotted line in Fig.7(c).

In Fig.7(d) the final section is compared with the NACA 0012 starting point. The final aerofoil is thicker than the original, 12.5% compared with 12% and the C_L has increased from 0.44 to 0.98 for roughly the same shock strength.

Finally in Fig.7(e) a comparison is presented of calculations for the final shape using the present small perturbation method and the nominally exact method of ref.5. The agreement is good.

For the second example of the application of the design method somewhat more ambitious targets are chosen. Initially a cusped thickness distribution with a t/c of 9% was taken and a subcritical design method was used to produce an initial approximation to the required shape. The pressure distributions obtained for this shape by forward calculation at a Mach number of 0.825 is shown as the solid line in Fig.8(a). A new upper surface pressure distribution was then specified - shown as the dashed line in Fig.8(a). The shock wave has been moved to beyond 80% chord and made quite weak. The design program was used to obtain this upper surface pressure distribution whilst maintaining the original thickness distribution. The design calculation was not taken to convergence as it became clear during its course that the lower surface velocity distribution would not be acceptable. The pressure distribution obtained by subsequent forward calculation is shown in Fig.8(b) - the solid line. As the design process was not taken to convergence this does not correspond to the required upper surface pressure distribution - shown once again by the dashed line. The section was then redesigned to obtain the same target upper surface velocities as before but in addition, a more acceptable lower surface target was specified (Fig.8(b)). Thus both lower surface and upper surface shapes were allowed to change with no direct control over thickness. This calculation was taken to convergence and forward calculation gave a virtually identical result.

The final aerofoil is depicted in Fig.8(c). According to the present calculation it produces a $C_L = 0.53$ at $M = 0.825$ with a very weak shock wave. It is 8.9% thick and has a base thickness of 1% chord.

Unfortunately it was not found possible to perform calculations using the Bauer, Garabedian & Korn program[5] at the design condition of this section. When the hyperbolic region extends to near the trailing edge of the aerofoil and far out from the surface the velocity vector may become non-aligned with the coordinate system and the zone of dependence of the difference scheme no longer includes that of the differential equation. This then leads to instability and divergence. This phenomenon is further discussed in Section 3.6. below.

A comparison of the pressure distributions obtained for the present method and by the Garabedian method at an off-design condition ($M = 0.79$) is shown in Fig.8(d). Bearing in mind that the forward shock should move from around 20% chord to 80% for a change in Mach number of 0.035, the agreement is good.

3. CALCULATION OF AXISYMMETRIC TRANSONIC FLOWS PAST BODIES OF REVOLUTION

3.1. Introduction

Both Bailey[10] and Murman and Krupp[2] have obtained solutions for the axisymmetric transonic flow past very slender bodies of revolution by methods analogous to the ones for aerofoils. Neither method is suited to the treatment of blunt nosed shapes which constitute a class of considerable practical interest. We would expect in any case that the use of an efficient coordinate system which accurately treats the nose region should not only provide more accurate solutions but also quicker ones.

The choice of coordinate system falls on that due to Sells[11,12] in which the region exterior to the profile is conformally mapped to the interior of the unit circle. Sells[12] showed this to be particularly suitable for subcritical aerofoil calculations. The BGKJ methods use the same coordinate system for their transonic aerofoil calculations, the mapping, however, being derived by somewhat different methods.

3.2. The basic equations

Once again we attack the equation for the velocity potential, in this case the exact equation for the full potential in the physical $z(x,y)$ plane is

$$\left(a^2 - \phi_x^2\right)\phi_{xx} + \left(a^2 - \phi_y^2\right)\phi_{yy} + \frac{a^2}{y}\phi_y - 2\phi_x\phi_y\phi_{xy} = 0$$

This differs from the equation for planar flow by the inclusion of the term in $1/y$.

The speed of sound a is given by

$$\frac{\phi_x^2 + \phi_y^2}{2} + \frac{a^2}{\gamma-1} = \frac{U_\infty^2}{2} + \frac{a_\infty^2}{\gamma-1}$$

The transformation to the $\sigma(r,\theta)$ computation plane is described by the modulus of the transform derivative

$$B = \left|\frac{dz}{d\sigma}\right|$$

In the σ plane the above equation then becomes

$$\left(a^2- u^2\right)\phi_{\theta\theta} + r^2\left(a^2- v^2\right)\phi_{rr} - 2ruv\,\phi_{\theta r} + \frac{a^2}{y}\frac{\partial y}{\partial\theta}\,\phi_\theta$$

$$+ r\,\phi_r\left(a^2+a^2\frac{r}{y}\frac{\partial y}{\partial r} + u^2\right) + r\left(u^2+ v^2\right)\left(rv\frac{\partial B}{\partial r} + u\frac{\partial B}{\partial\theta}\right) = 0$$

where $u = \phi_\theta/Br$, $v = \phi r/B$ are the velocity components in the θ and r directions.

The singularities in ϕ and B at r = 0 (corresponding to infinity in the physical plane) are removed by introducing the reduced potential Φ

$$\Phi = \phi - \cos\theta/r$$

and $$f = Br^2$$

the governing equation then becomes

$$\left(a^2- u^2\right)\Phi_{\theta\theta} - 2ruv\,\Phi_{r\theta} + r^2\left(a^2- v^2\right)\Phi_{rr} + \left(\frac{a^2}{y}\frac{\partial y}{\partial\theta} - 2uv\right)\Phi_\theta$$

$$+ r\left(a^2+ \frac{a^2r}{y}\frac{\partial y}{\partial r} + u^2 - 2v^2\right)\Phi_r + f^{-1}\left(u^2+ v^2\right)\left(r^2f_r\Phi_r + f_\theta\Phi_\theta\right)$$

$$= \frac{a^2}{y}\frac{\partial y}{\partial r}\cos\theta + \frac{a^2}{ry}\frac{\partial y}{\partial\theta}\sin\theta + \frac{f^{-1}}{r}\left(u^2+ v^2\right)\left(rf_r\cos\theta + f_\theta\sin\theta\right)$$

which is the equation we use.

3.3. Mapping

Both the transform derivative and y, the radius in the physical plane, are required at points within, and on the surface of, the unit circle.

We use the mapping due to Catherall,Foster and Sells[11] which is directly valid for blunt nosed bodies with pointed, rounded or open tails. In the case of open bodies the "sting" is mapped to the line θ = 0 in the computational plane (see Fig.9), the "sting"/body junction being mapped to r = 1, θ = 0. By using a small (and in this

context irrelevant) amount of nose rounding, bodies with pointed noses may also be treated.

The Catherall-Foster-Sells method conveniently supplies the B and y on the surface of the circle. Values on the inside of the circle can be calculated by the use of Poisson's integral.

In order to use this we put

$$y' = y + \frac{\sin\theta}{r} + y_s \left(1 - \frac{\theta}{\pi}\right)$$

$$J = \ell nB + 2\ell nr - k\left(\tfrac{1}{2}\ell n\,(1-2r\cos\theta+r^2) + r\cos\theta\right)$$

where $k = 1 - \delta/\pi$, δ is the trailing edge angle and y_s is the sting diameter

to remove all singularities at the tail, along $\theta = 0$ and at $r = 0$. The Poisson integral is

$$f(re^{i\theta}) = \frac{1}{2\pi} \int_0^{2\pi} \frac{1 - r^2}{1-2r\cos(\theta-\phi) + r^2} f(e^{i\phi})\, d\phi$$

which when written in the form

$$f(re^{i\theta}) = f(e^{i\theta}) + \frac{1}{2\pi} \int_0^{2\pi} \frac{(1 - r^2)}{1-2r\cos(\theta-\phi)+r^2} \left[f(e^{i\phi}) - f(e^{i\theta})\right] d\phi$$

is suitable for any simple numerical integration routine.

The geometric terms $\frac{1}{y}\frac{\partial y}{\partial \theta}$ and $\frac{1}{y}\frac{\partial y}{\partial r}$ in the partial differential equation are calculated by simple finite differences.

3.4. Boundary conditions

3.4.1. Body surface ($r = 1$)

Here $\phi_r = 0$, $\Phi_r = \cos\theta$. This may be conveniently incorporated in the difference scheme via the expression for Φ_{rr}.

3.4.2. Axis of symmetry ($\theta = 0, \pi$; $r < 1$)

Terms originating from the $\frac{1}{y}\phi_y$ expression in the basic equation for axisymmetric flow tend to certain limits on the axis of symmetry. Referring to the equation for the full potential ϕ at the top of page 16 we have as $\theta \to 0,\pi$

$$\frac{1}{y}\frac{\partial y}{\partial \theta}\phi_\theta \to \frac{\partial y}{\partial \theta}\frac{\partial}{\partial \theta}(\phi_\theta) \Big/ \frac{\partial}{\partial \theta}(y)$$

$$\to \phi_{\theta\theta}$$

$$\frac{1}{y}\frac{\partial y}{\partial r} \to \frac{\partial^2 y}{\partial r^2} \Big/ \frac{\partial y}{\partial r}$$

and also $u, \frac{\partial B}{\partial \theta} \to 0$

3.4.3. Leading and trailing edges ($\theta = 0,\pi$; $r = 1$)

At these points the velocity components vanish

i.e. $u = v = 0$

and the equation for the full potential reduces to that of Laplace

$$\phi_{\theta\theta} + r^2\phi_{rr} + \frac{1}{y}\frac{\partial y}{\partial \theta}\phi_\theta + r\left[1 + \frac{r}{y}\frac{\partial y}{\partial r}\right]\phi_r = 0$$

At the nose and tail of closed bodies $r = 1$, $y = 0$ and so the equation further reduces to

$$2\phi_{\theta\theta} + \phi_{rr} = 0$$

For open tailed bodies,at the body/"sting" junction $y \neq 0$ and the equation reduces to

$$\phi_{\theta\theta} + \phi_{rr} = 0.$$

3.4.4. Far field ($r = 0$)

As $z \to \infty$ $\phi \to x$, $x \to \frac{\cos\theta}{r}$

hence $\Phi = 0$

which is easily incorporated in the difference equations.

3.5. Difference schemes

We adopt almost without change the difference scheme used in the GKBJ methods. Following Murman they march from the nose to the tail

of the body solving the difference equations by line over-relaxation. At each point all first derivatives are "frozen" i.e. they are calculated using values from the previous sweep through the field. Central differences are used for first derivatives and for the approximation to Φ_{rr}.

If the flow at any point is subsonic, $u^2 + v^2 < a^2$, the second derivatives involving θ are calculated using central differences. For the hyperbolic region a second order accurate version of Murman's method is obtained by setting

$$(\Delta\theta^2)\Phi_{\theta\theta} \quad (\Phi_{j,k} - 2\Phi_{j-1,k} + \Phi_{j-2,k}) + \varepsilon\,(\Phi_{j,k} - 3\Phi_{j-1,k} + 3\Phi_{j-2,k} - \Phi_{j-3,k})$$

where $\quad 0 \leq \varepsilon < 1$

with a similar expression for $\Phi_{\theta r}$.

This gives a difference scheme which is second order accurate if $\varepsilon > 0$ and which is stable for sufficiently small ε because of a favourable artificial viscosity. From experience with the GKBJ methods we would expect that using $\varepsilon = 0$ will give sufficient accuracy in most cases, apart from those displaying near shock free recompressive conditions. These are in any case less commonly found in bodies of revolution than on aerofoils.

3.6. Limitations of present difference scheme

The present hyperbolic difference scheme is limited to cases where the velocity vector is nearly aligned with the θ direction. The Sells mapping is successful in providing this condition for cases where the hyperbolic region is confined to the centre part of the body and does not extend too far from it. As the free stream Mach number increases and the supersonic region becomes of greater extent, the velocity vector may become non-aligned with the θ direction and at some points

$$u^2,\ v^2 < a^2 < u^2 + v^2$$

i.e. the velocity components are subsonic but the flow is supersonic. If too many points obey this inequality then instability will result

because firstly the diagonal dominance of the implicit scheme is lost and secondly the zone of dependence of the difference scheme no longer includes that of the differential equation. This is shown diagrammatically in Fig.(10).

Jameson[13] has suggested a difference scheme which remedies this situation. At each point in the field the difference scheme is rotated to conform with the local flow direction. This eliminates any need to align one of the coordinates with the local flow direction.

Jameson has used the scheme for both two and three dimensional calculations and South[14] has used it for axisymmetric flows. One important advantage of the Jameson method is that it makes possible calculation with supersonic free streams if it is combined with a coordinate system which is capable of representing the flow at infinity correctly.

We intend that at a later stage a rotated difference scheme should be incorporated in the present method but it is doubtful that calculations with supersonic free streams will be possible with the Sells transformation.

3.7. Computer program

The method described has been programmed in Fortran. Mesh refinement is used as described in the first part of the paper. Most calculations are done with a fine grid having 60 x 20 points in the half circle. This is somewhat coarser than that used in the GKBJ methods but is sufficiently accurate in most cases. Computation times per mesh point are somewhat larger than the corresponding two dimensional case. About 100 iterations are usually required on the fine grid which takes about ½ minute on a CDC 6600 computer.

3.8. Examples

3.8.1. Ellipsoid

The first example is that of an ellipsoid of fineness ratio, L/D≒3.6 generated by Joukowski transformation from the unit circle with singular points at $\pm$0.75. Figure 11(a,b) show the surface pressure distributions for progressively increasing Mach numbers up to 0.95. Some of the results are compared with calculations by Jameson[7]. The agreement is quite good especially at the highest Mach number. At this point the peak local Mach number is about 1.3.

3.8.2. Body with blunt nose and pointed tail

This body, shown in Fig.12, was generated by rotating a symmetric Karman-Trefftz aerofoil about its axis of symmetry. The fineness ratio L/D, is 4.74, and total included angle at the tail is 25.95°.

Calculations for this type of body have proved to be very difficult. With the method as described it was only possible to reach a freestream Mach number of 0.8 and this only by using very small increments in Mach number. The failure is caused by large disturbances starting at the tail and gradually moving forward until complete breakdown is produced.

This behaviour can be plausibly explained by comparing the behaviour of the velocity potential near the tip of a wedge and a circular cone in incompressible flow.

Taking ζ as the ordinate along the surface then for both cases $\phi \propto \zeta^{\nu}$

where ν is a function of cone or wedge angle. The variation of ν with wedge/cone angle is shown in Fig.13. Note that the power law behaviour is the same in axisymmetric and plane flow for cusped and blunt tails. When the wedge is unwrapped by conformal transformation into a half plane

(locally near the tail similar to our mapping the entire profile into a circle) the potential behaves like a simple stagnation point flow $\phi \propto \xi^2$ (the ζ direction having mapped into the ξ direction). For a cone the behaviour is not so simple except for cusped or blunt tails.

Thus the behaviour of the velocity potential near a pointed tail is more complicated than in the planar case and may not be adequately represented by simple difference schemes.

The situation is almost certainly made worse by the fact that the direction of sweeping in the calculation tends to push "errors" into the tail region where the symmetry boundary conditions tend to magnify them making any inaccuracies in this region worse.

In view of these arguments we have attempted to overcome the problem by matching the calculated solution very close to the tail to the solution for the incompressible flow past a cone. This certainly leads to considerable improvements for subcritical calculations in that it is no longer necessary to proceed in small steps in Mach number. However it is still not possible to proceed into the transonic regime by any significant amount.

Figure 14(a) shows pressure distributions calculated for this body obtained both with and without a matched cone solution at the rear; on this scale the differences between the two sets of results are not discernable. In 14(b) a slightly supercritical calculation is shown, obtained using a matched cone solution.

3.8.3. Hemisphere-cylinder

The singular point of the transformation was placed 1.5 diameters downstream of the nose. For the case of a continuous cylindrical afterbody the boundary conditions at the singular point of the transformation are not correct as this point is assumed to be a stagnation point. The effect of this error is very local however and is

not expected to have any serious effect in the region of interest near the nose. Calculations for this body are shown in Fig.15 for Mach numbers from 0.1 to 0.75.

It was hoped that it would be possible to compare these calculations with experiment, as the body concerned is one of practical importance because of its use as a pitot-static head. However the only experimental evidence which could be found[15] was obtained at low Reynolds number without boundary layer transition fixing. The measured pressure distributions are thus dominated by shock wave - boundary layer interaction and provide no suitable comparison with the inviscid theory.

3.8.4. Ogive-cylinder

The problems of calculating the flow past a body with a pointed tail have already been discussed. The problems for sharp noses do not seem so acute, probably because of the direction of sweeping in the calculation. For the case in question, an ogive cylinder with nose length equal to the maximum diameter, it was necessary to round the nose slightly in order to perform the mapping. This may have had some beneficial effect on the convergence of the calculations.

Experimental results for this body in combination with a short conical boattail are given in Reference 16 and is designated configuration 5. We have made no allowance for the effect of the boattail. Figures 16(a,b,c) show a comparison of the calculation with the experimental results for three Mach numbers, 0.4, 0.6 and 0.83. The agreement is very good.

4. CONCLUSIONS

Two methods have been presented for the calculation of transonic flows. Both are logical developments of the relaxation methods first developed by Murman and his associates.

The first method is for the design of aerofoils with specified pressure distributions including shock waves. This has been developed from the Murman-Krupp method for the solution of the transonic small perturbation equation with linearized boundary conditions. Examples of its use have been given and its value for the design of supercritical aerofoils demonstrated.

The second method which has been described is for the calculation of axisymmetric transonic flows past bodies of revolution. In this case the exact potential flow equations have been solved in a manner similar to that used by Garabedian et al for planar calculations. The calculation of flows with strong shock waves for bodies with pointed tails has not been successful but for other bodies excellent results have been obtained.

ACKNOWLEDGEMENTS

Finally, the author wishes to thank Miss M.J.Evans and Mr.C.R.Forsey who did the majority of the work presented in this paper.

REFERENCES

1. Murman, E.M. Cole, J.D. — Calculation of plane steady transonic flows. AIAA Journal, Vol.9, pp.114-121. (1971).

2. Murman, E.M. Krupp, J.A. — The numerical calculation of steady transonic flows past thin lifting aerofoils and slender bodies. AIAA Journal, Vol.10, pp.880-886. (1972).

3. Krupp, J.A. — The numerical calculation of plane steady transonic flows past lifting aerofoils. Boeing Scientific Research Lab. paper D180 - 12958-1. (1971).

4. Nieuwland, G.Y. — Transonic potential flow around a family of quasi-elliptical aerofoil sections. NLR TR R-172.

5. Bauer, F. Garabedian, P.R. Korn, D.G. — Supercritical wing sections. (Lecture notes in economics and mathematical systems No.66). Springer-Verlag Berlin. (1972).

6. Garabedian, P.R. Korn, D.G. — Analysis of transonic aerofoils. Comm. Pure Appl. Math. Vol.24. (1972).

7. Jameson, A. — Transonic flow calculations for airfoils and bodies of revolution. Grumman Aerodynamic Report 390-71-1. (1971).

8. Kacprzynski, J.J. Ohman, L.H. Garabedian, P.R. Korn, D.G. — Analysis of the flow past a shockless lifting aerofoil in design and off design conditions. NRC Aero Report LR-554. (1971).

9. Steger, J.L. Klineberg, J.M. — A finite difference method for transonic aerofoil design. AIAA Journal, Vol.11, pp.628-635. (1973).

10. Bailey, F.R. — Numerical calculation of transonic flow about slender bodies of revolution. NASA TN D-6582. (1971).

11. Catherall, D. Foster, D.N. Sells, C.C.L. — Two dimensional incompressible flow past a lifting aerofoil. RAE TR 69118. (1969).

REFERENCES (Continued)

12.	Sells, C.C.L.	Plane subcritical flow past a lifting aerofoil. RAE TR 67146. (1967).
13.	Jameson, A.	Iterative solution of transonic flows over aerofoils and wings, including flows at Mach 1. Comm. Pure Appl. Math. To be published.
14.	South, J.C. Jameson, A.	Relaxation solutions for inviscid axisymmetric transonic flow over blunt or pointed noses. AIAA Computation Fluid Dynamics Conference. (1973).
15.	Rogers, E.W.E. Hall, I.M.	Wall interference at transonic speeds on a hemisphere cylinder model. ARC CP No.510. (1959).
16.	Fox, C.H.	Experimental surface pressure distributions for a family of axisymmetric bodies at subsonic speeds. NASA TM X-2439. (1971).

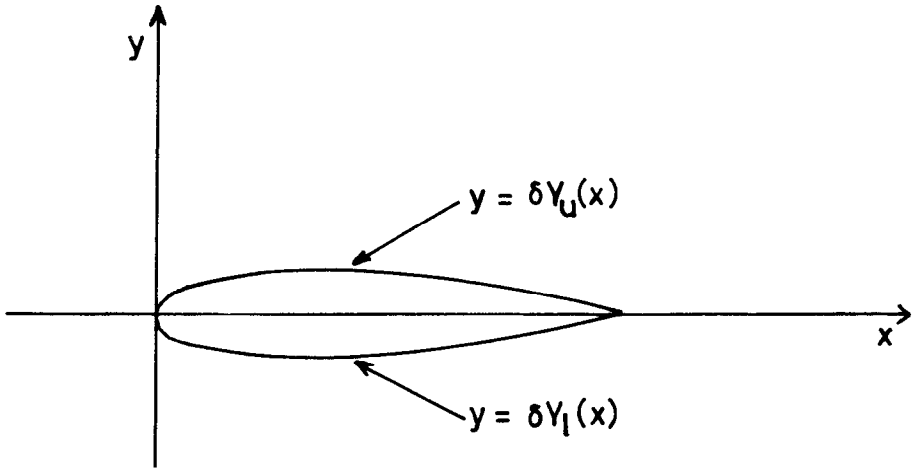

FIG.1 AEROFOIL GEOMETRY FOR SMALL PERTURBATION CALCULATIONS.

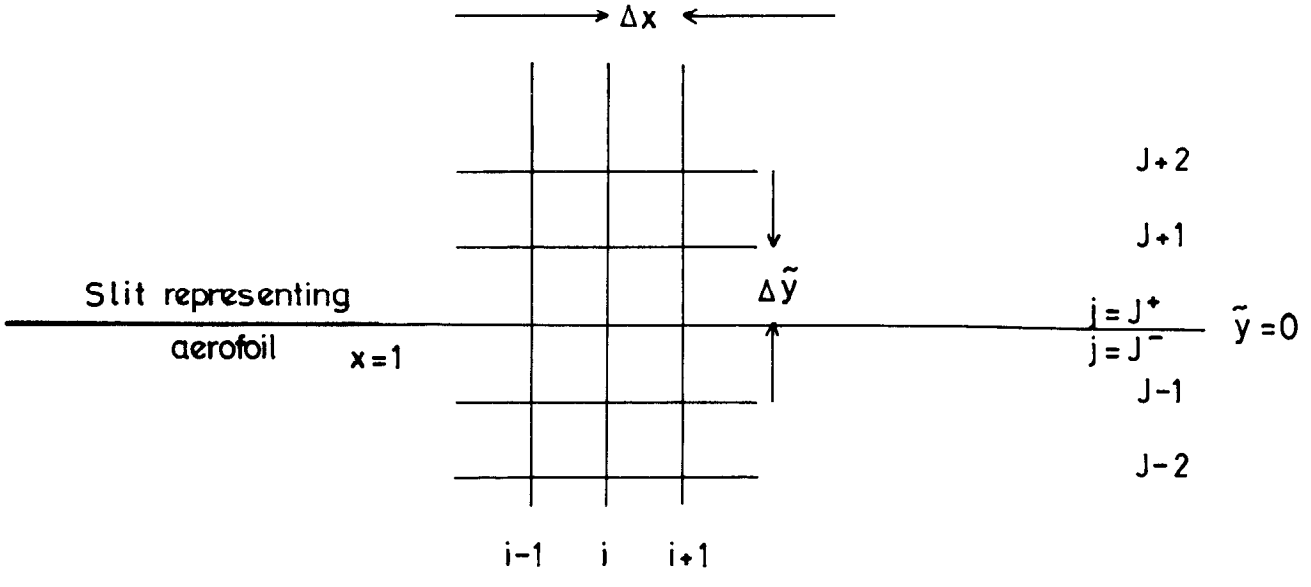

FIG. 2 NOMENCLATURE FOR DIFFERENCE SCHEME ACROSS SLIT DOWNSTREAM OF AEROFOIL.

FIG. 3

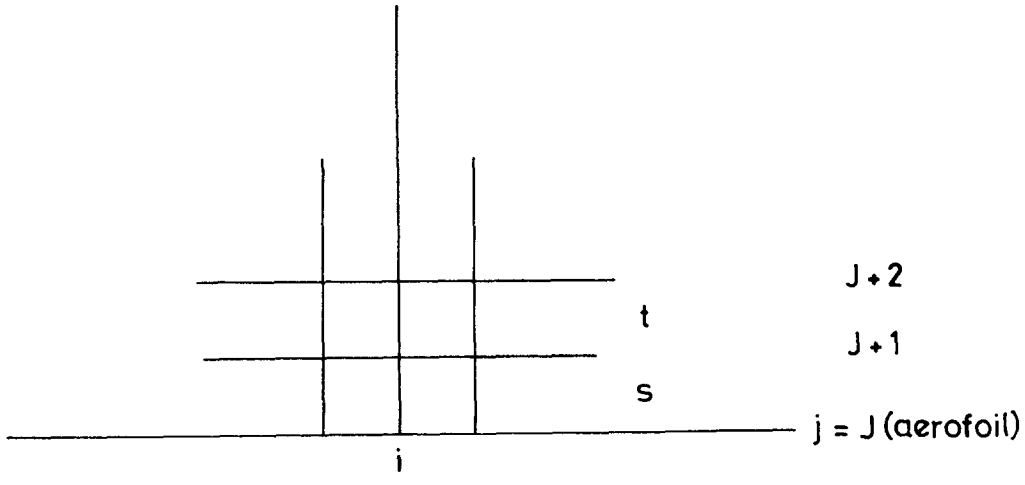

KRUPP SCHEME

$$\Phi_{\tilde{y}\tilde{y}/i,J+1} = \frac{2}{t(t+2s)}\left[\Phi_{i,J+2} - \Phi_{i,J+1}\right] - \frac{2}{(t+2s)}\Phi_{\tilde{y}/i,J} + \frac{(t^2/3 - s^2)}{(t+2s)}\Phi_{\tilde{y}\tilde{y}\tilde{y}/i,J} \cdots\cdots$$

$$\Phi_{i,J} = \Phi_{i,J+1} - \frac{s}{t}\left[\Phi_{i,J+2} - \Phi_{i,J+1}\right]$$

Errors minimized when $s = t/\sqrt{3}$

PRESENT SCHEME

$$\Phi_{\tilde{y}\tilde{y}/i,J} = \frac{2}{s^2}\left[\Phi_{i,J+1} - \Phi_{i,J} - s\Phi_{\tilde{y}/i,J} - \frac{s^3}{3!}\Phi_{\tilde{y}\tilde{y}\tilde{y}} \cdots\cdots\right]$$

Errors minimized when $s \rightarrow 0$

Other considerations require $s = t$

FIG.3 COMPARISON OF AEROFOIL BOUNDARY CONDITIONS.

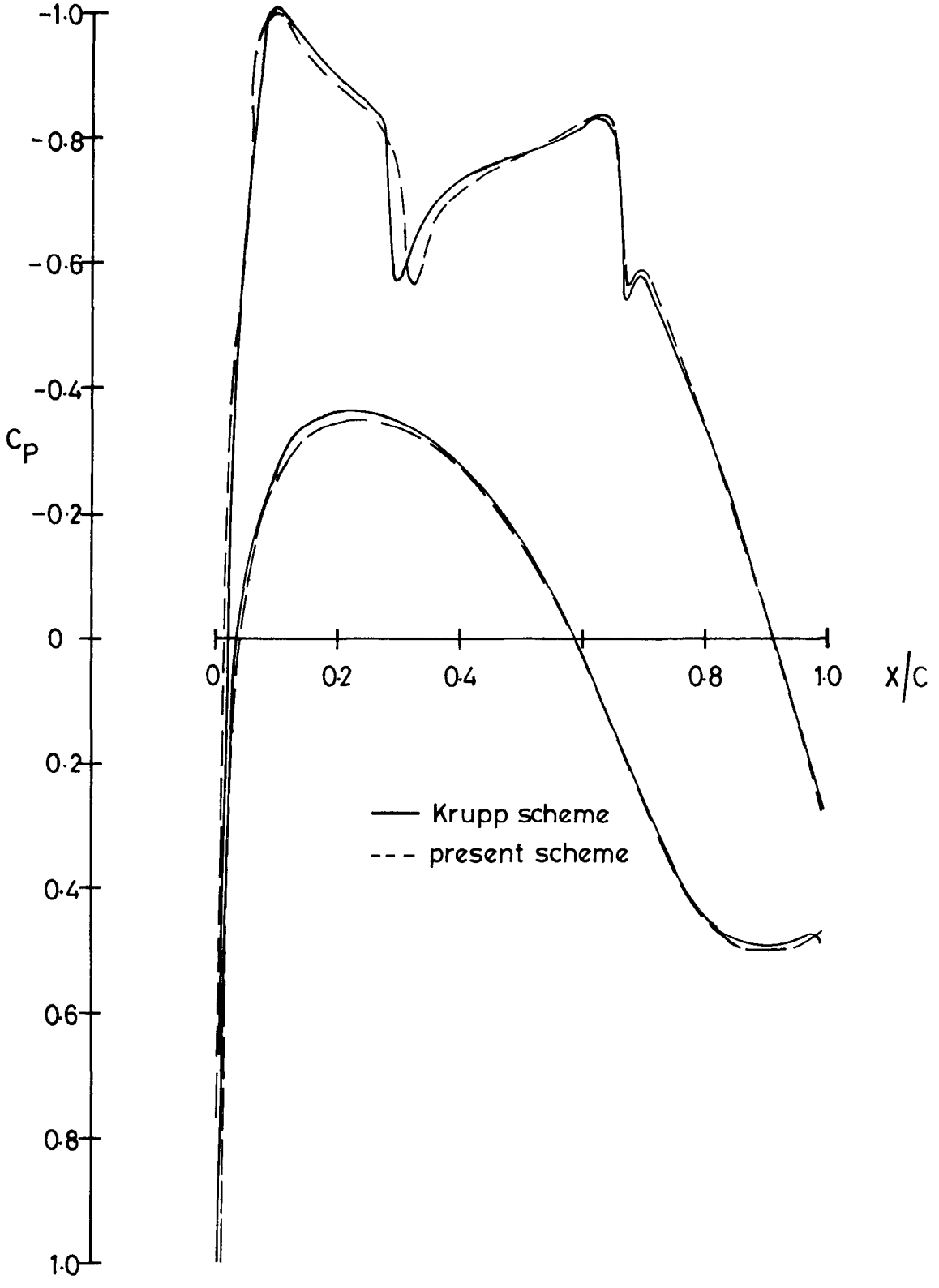

FIG. 4 COMPARISON OF CALCULATIONS USING DIFFERENT AEROFOIL BOUNDARY CONDITIONS

FIG. 5

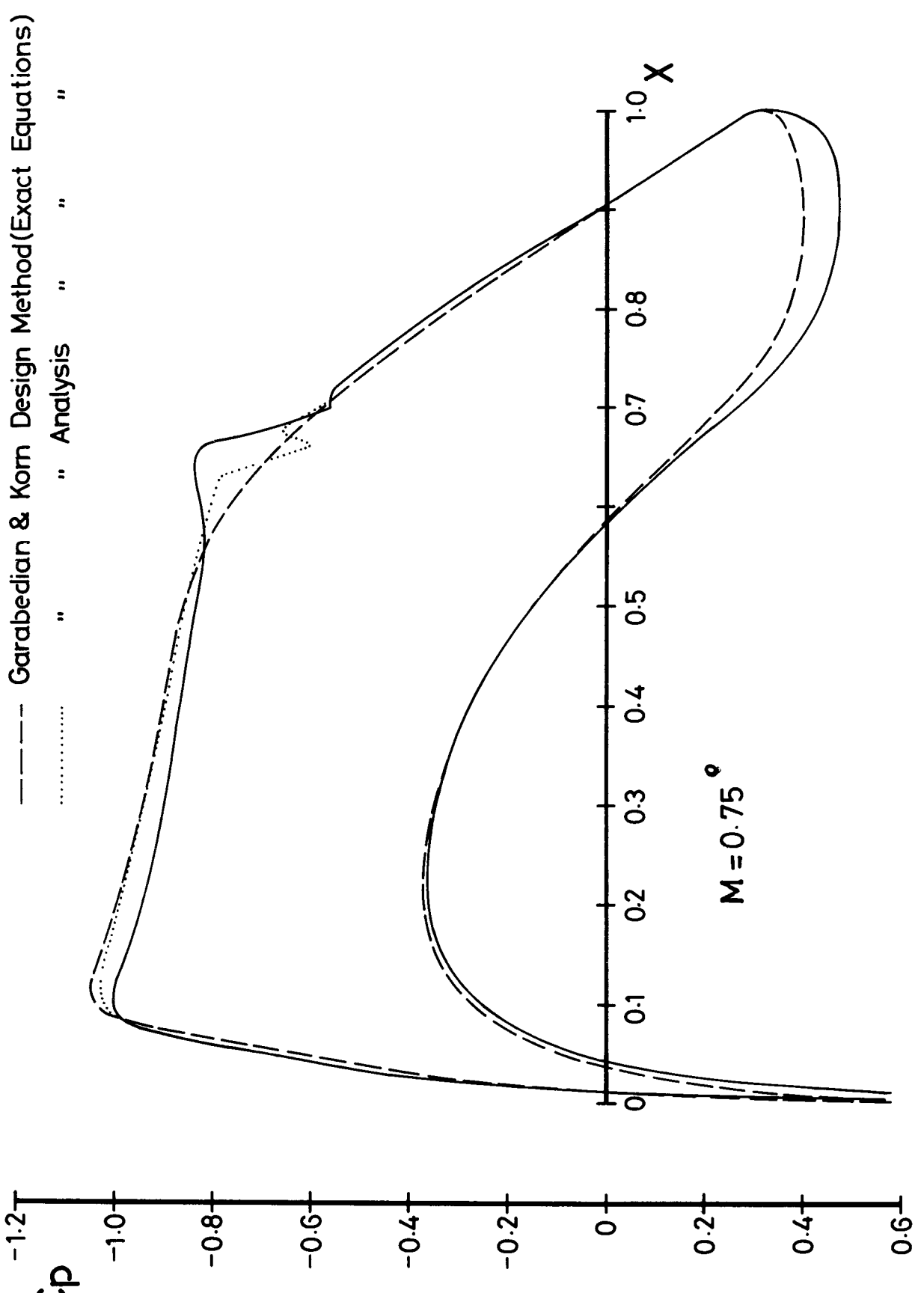

KORN AEROFOIL - COMPARISON OF DIFFERENT METHODS

FIG. 5

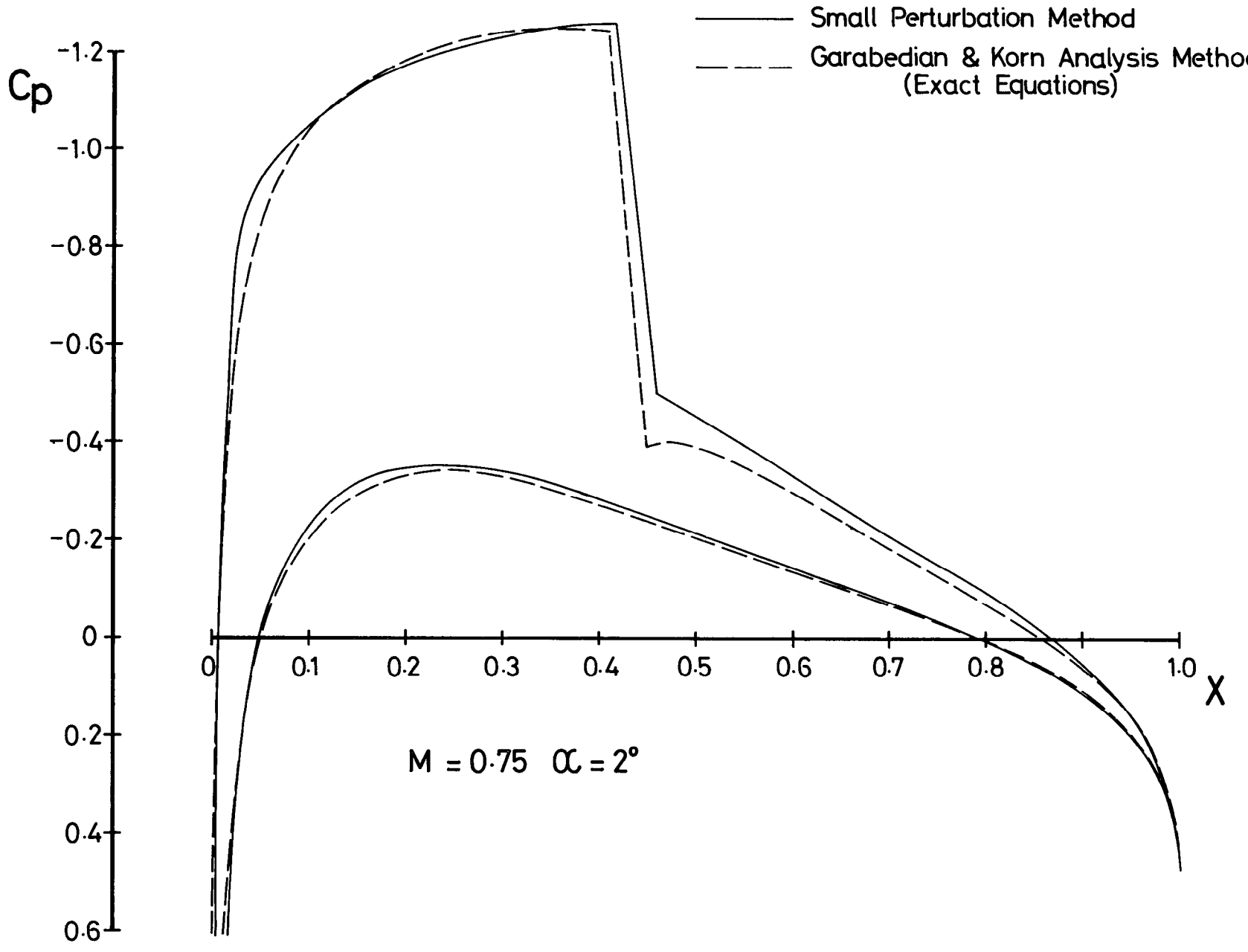

FIG. 6

N.A.C.A. 0012 - COMPARISON OF DIFFERENT METHODS

FIG. 6

FIG 7(a)

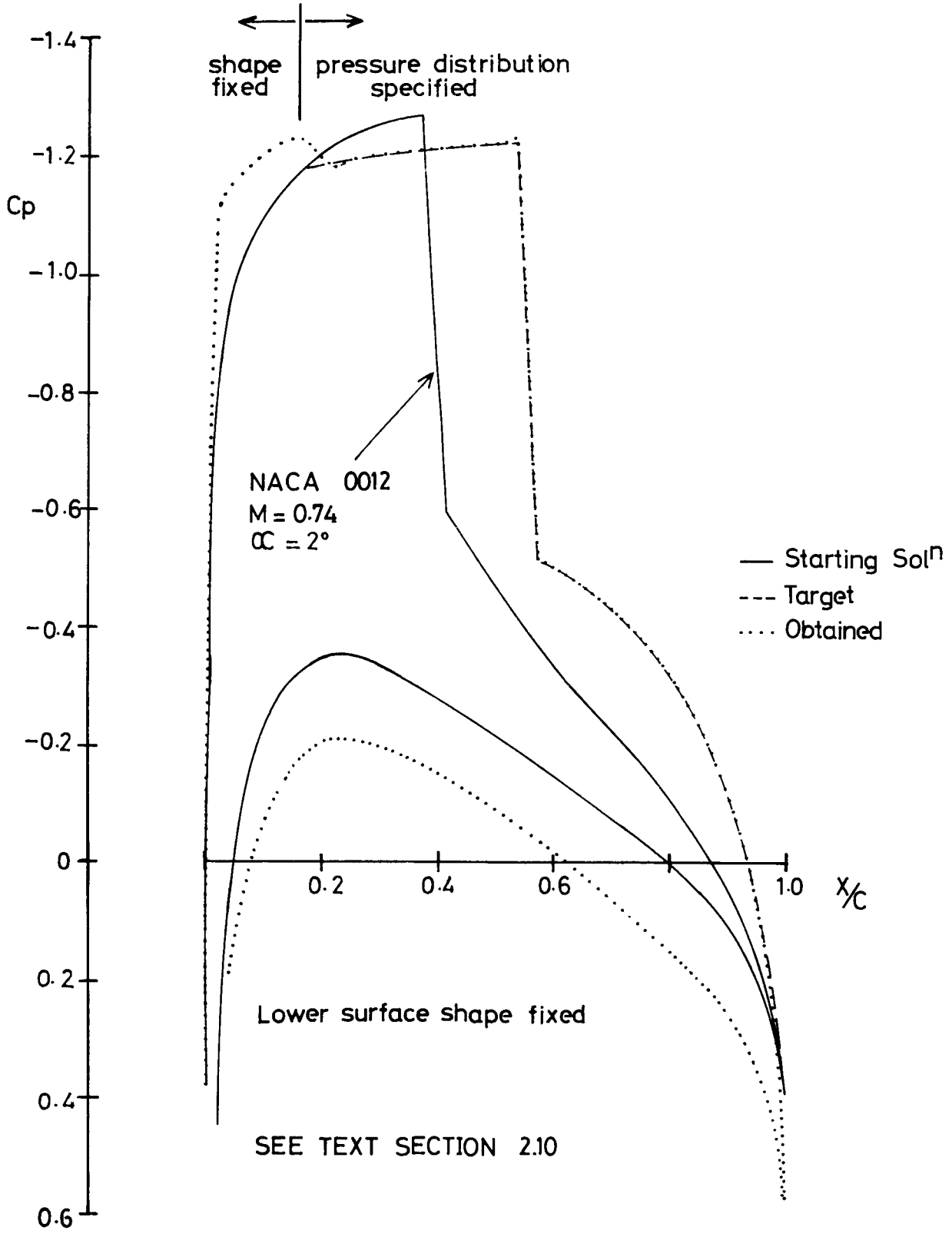

FIG 7(a) DESIGN BASED ON NACA 0012 - STAGE 1

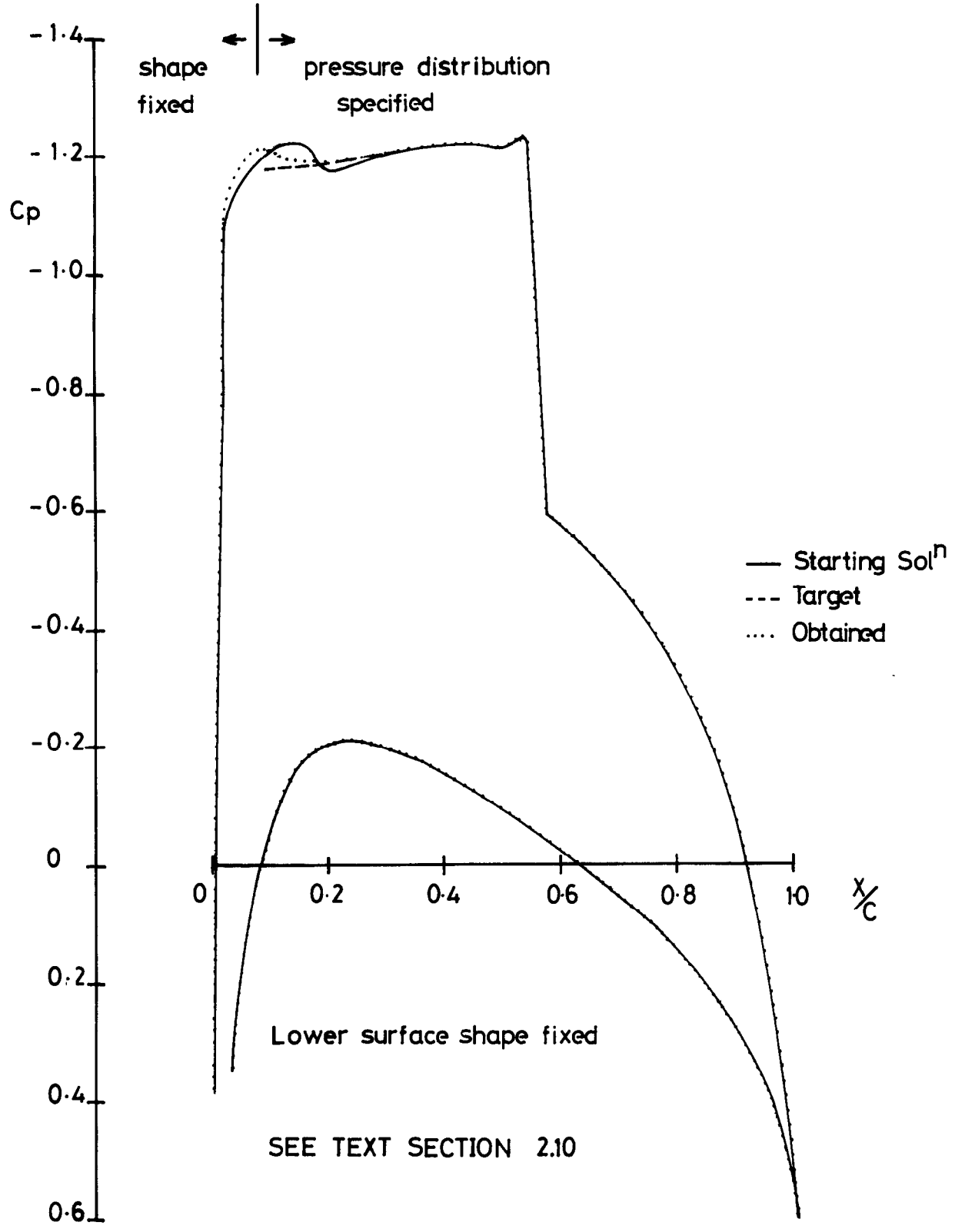

FIG 7(b) DESIGN BASED ON NACA 0012 - STAGE 2.

FIG. 7(c)

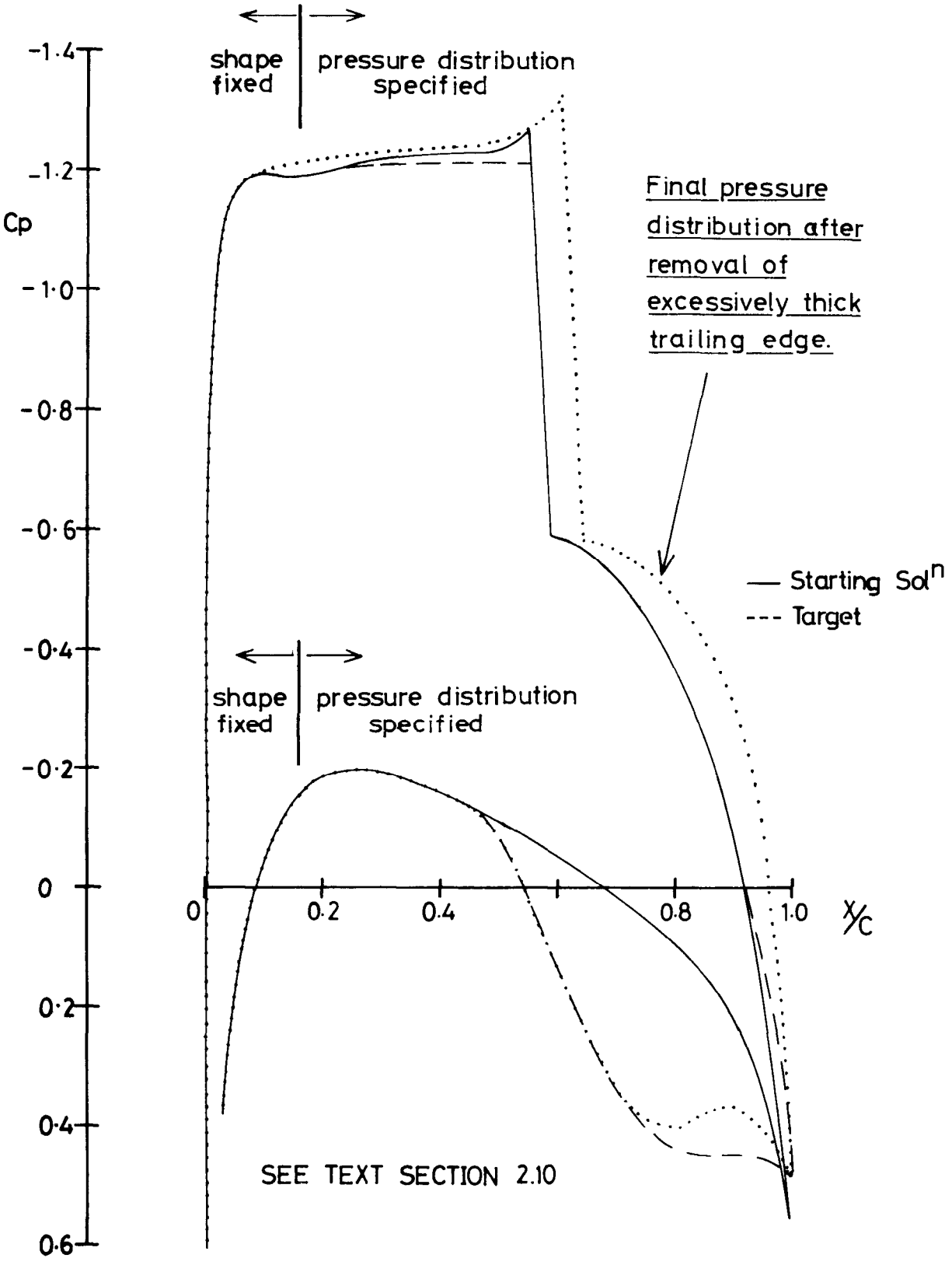

FIG 7(c) DESIGN BASED ON NACA 0012 - STAGE 3.

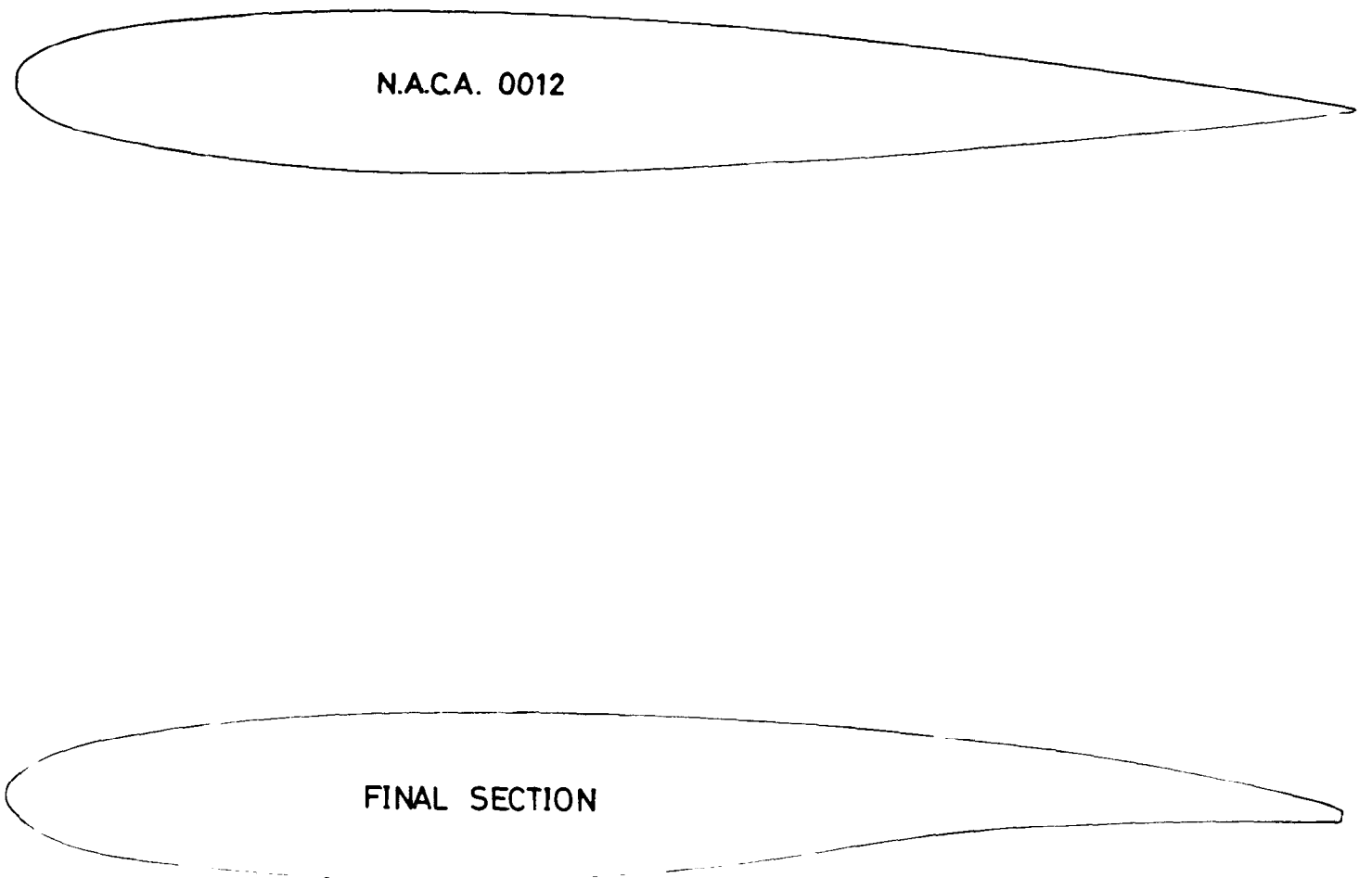

FIG. 7(d) DESIGN BASED ON N.A.C.A. 0012 - COMPARISON OF INITIAL AND FINAL SECTIONS

FIG 7(d)

FIG 7(e)

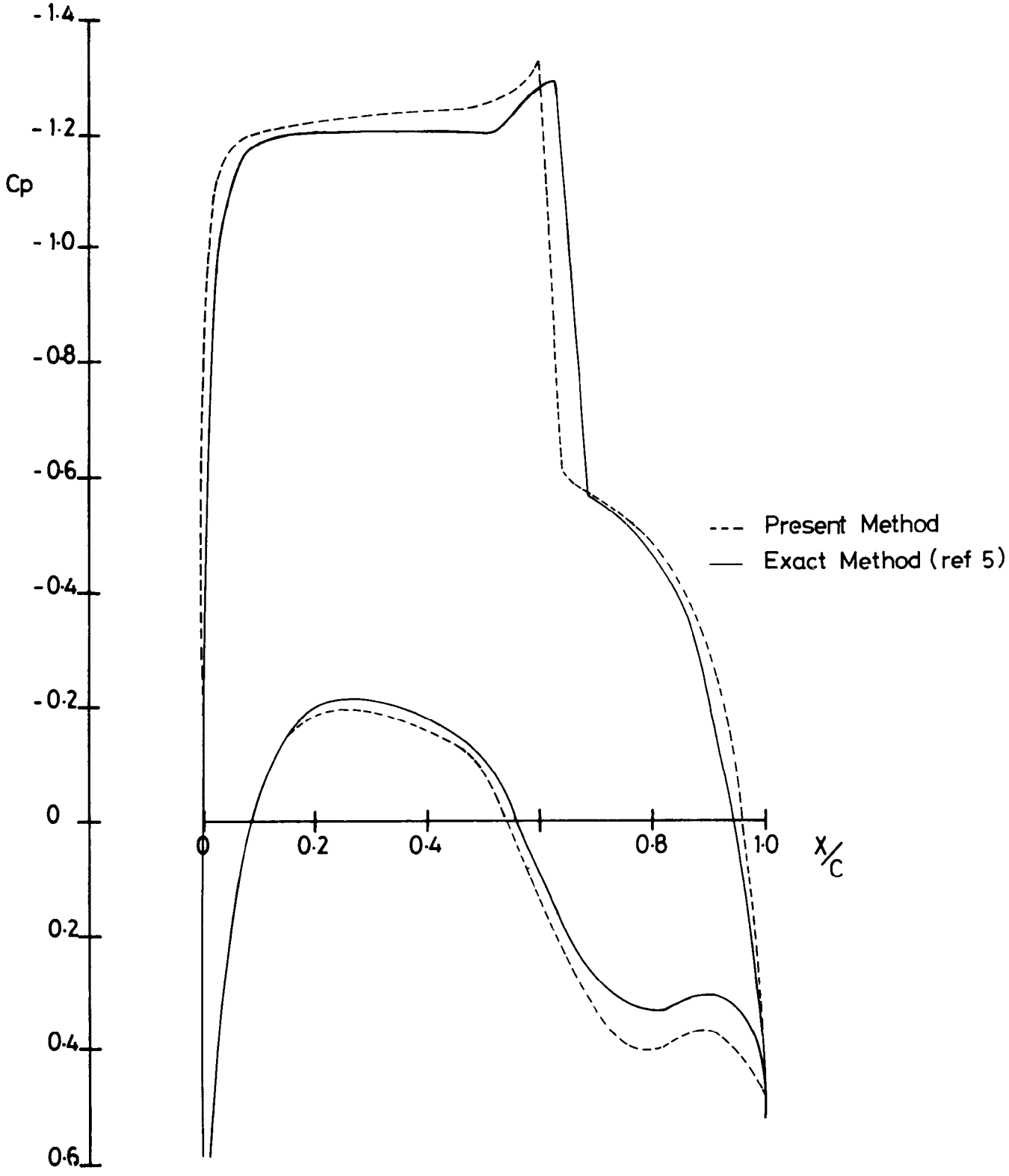

FIG. 7(e) DESIGN BASED ON NACA 0012 - COMPARISON WITH EXACT METHOD.

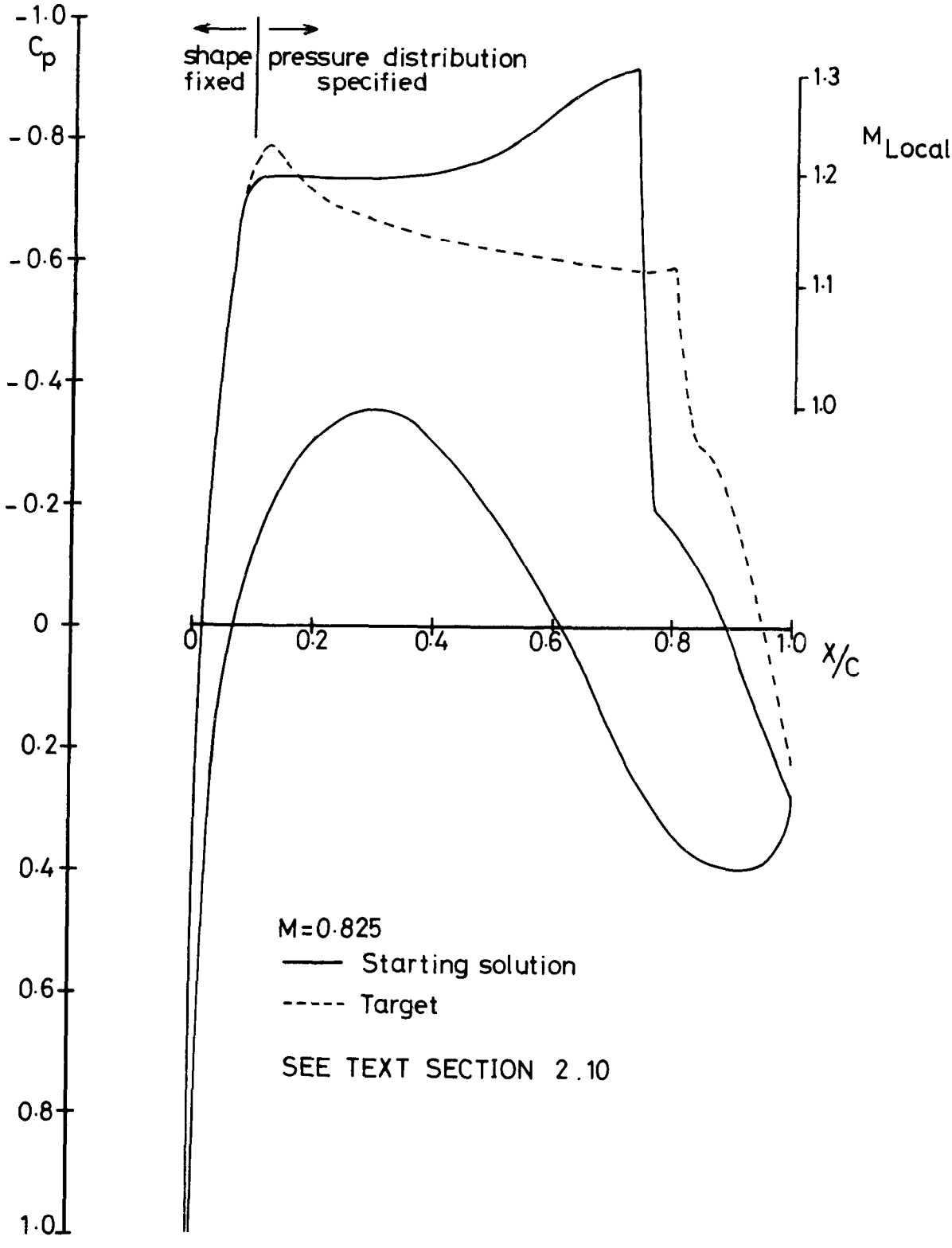

FIG. 8(a) DESIGN OF ADVANCED SECTION - STAGE 1

FIG. 8(b)

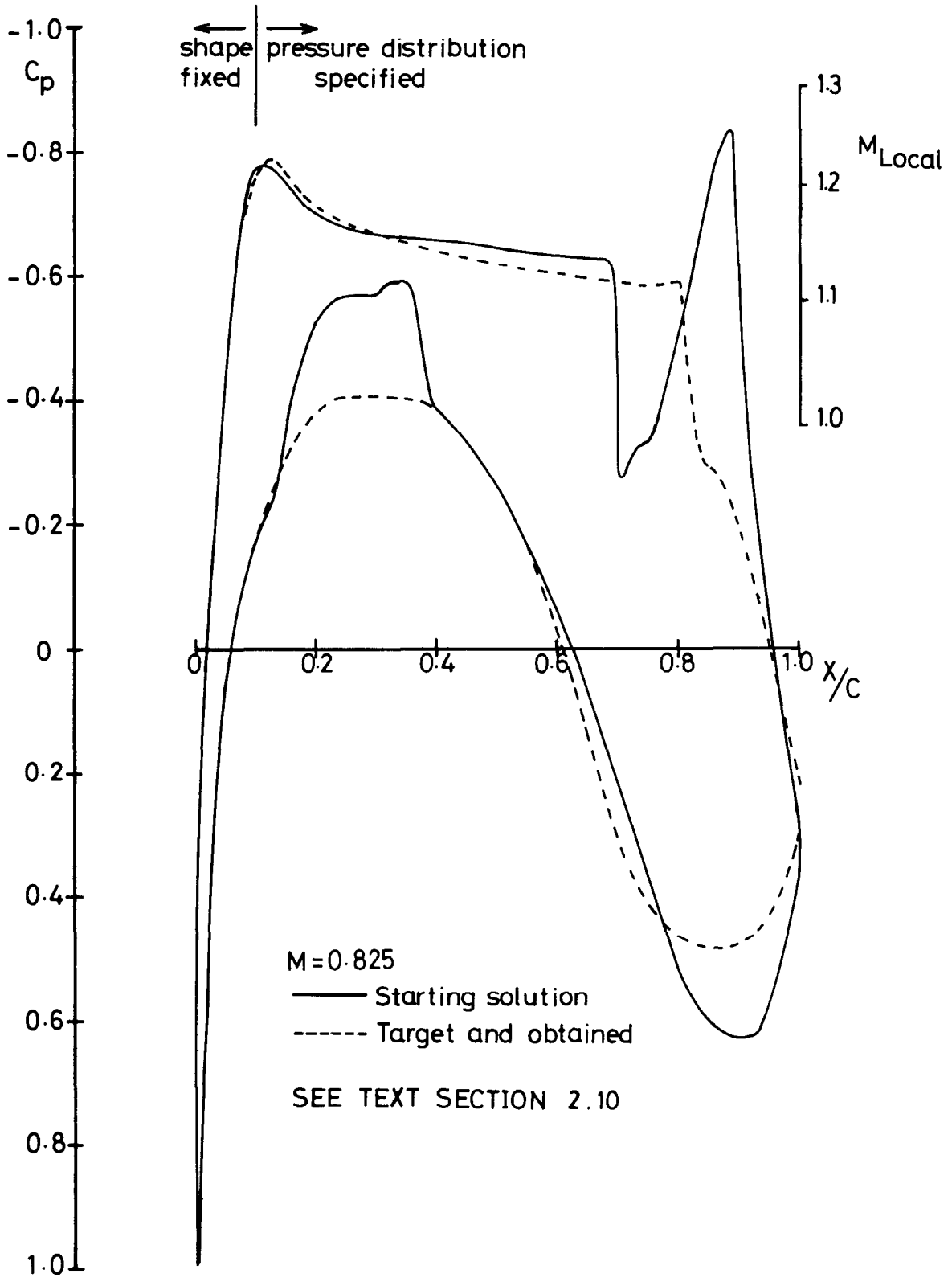

FIG. 8(b) DESIGN OF ADVANCED SECTION - STAGE 2

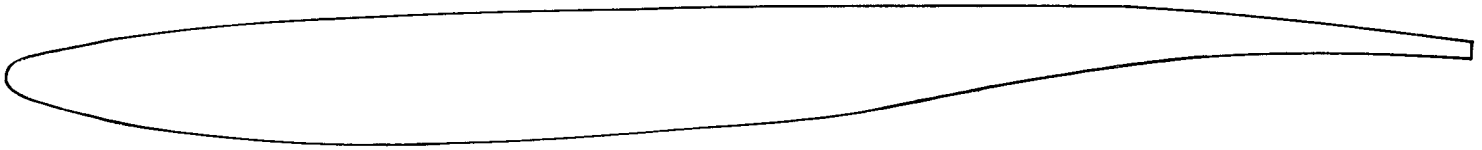

FIG. 8(c).

FIG. 8(c). DESIGN OF ADVANCED SECTION - FINAL SHAPE.

FIG. 8(d)

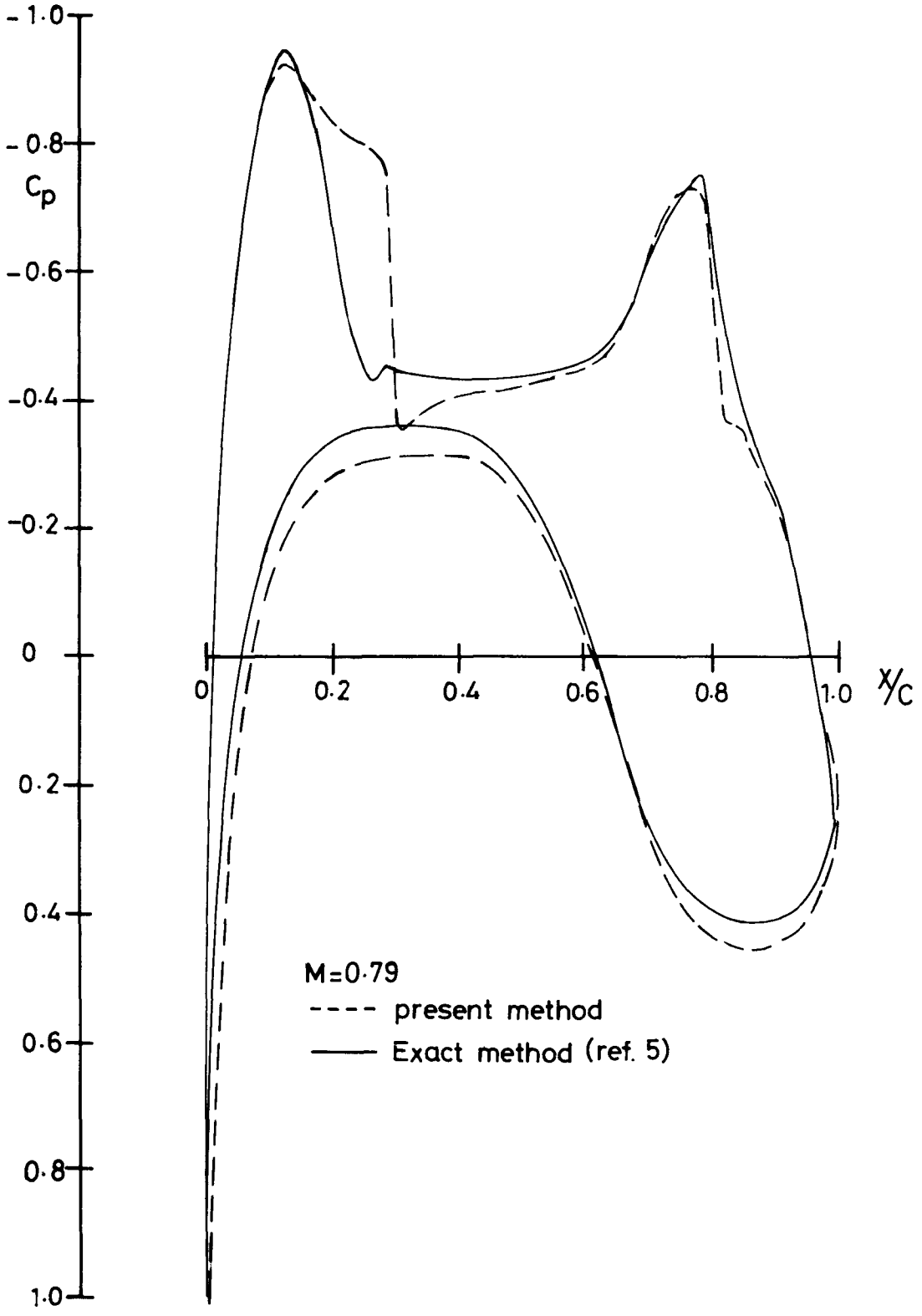

FIG. 8(d) DESIGN OF ADVANCED SECTION - COMPARISON WITH EXACT METHOD

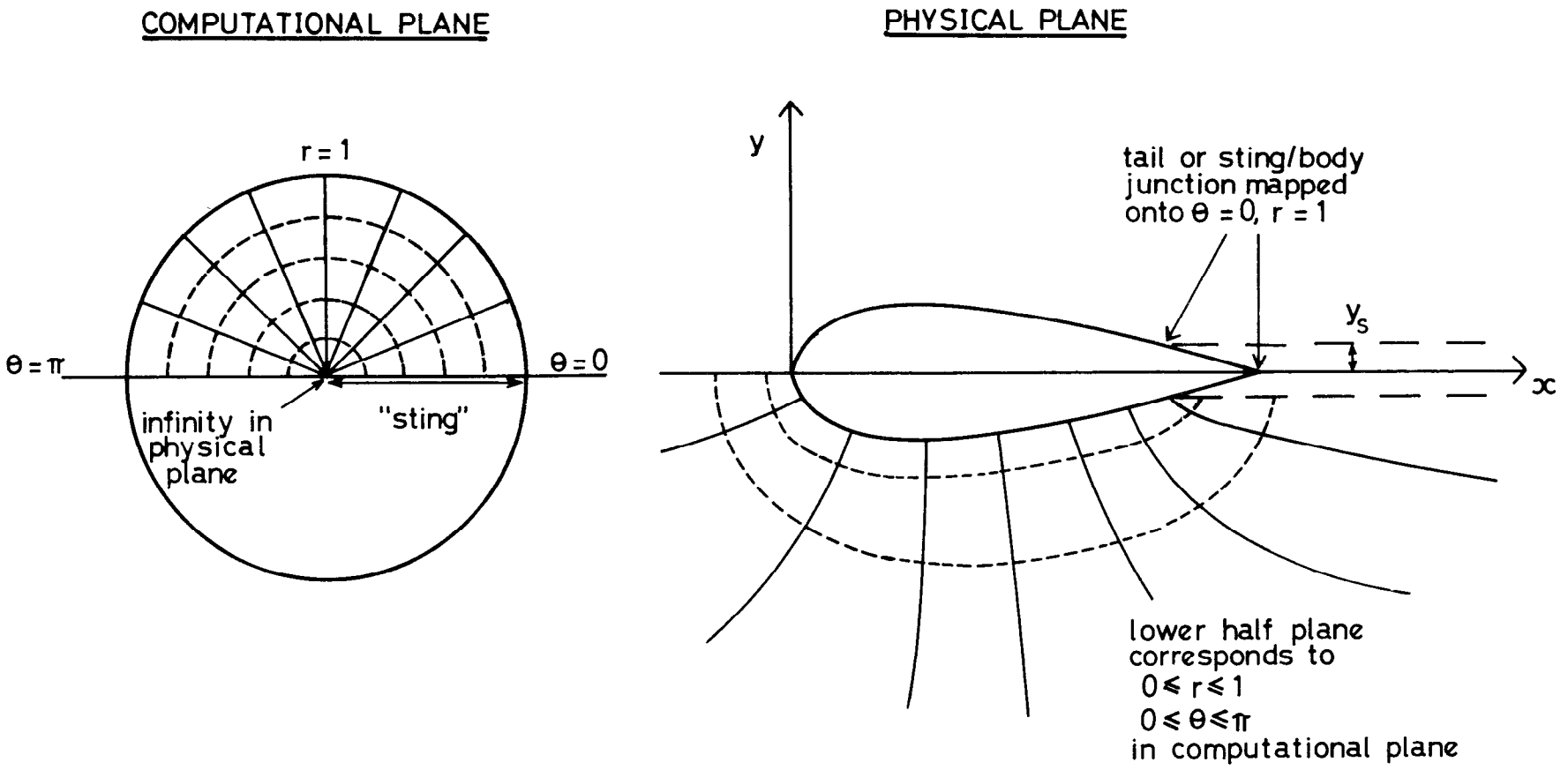

FIG. 9

FIG. 9 CO-ORDINATE SYSTEM FOR AXISYMMETRIC FLOW CALCULATIONS

FIG. 10

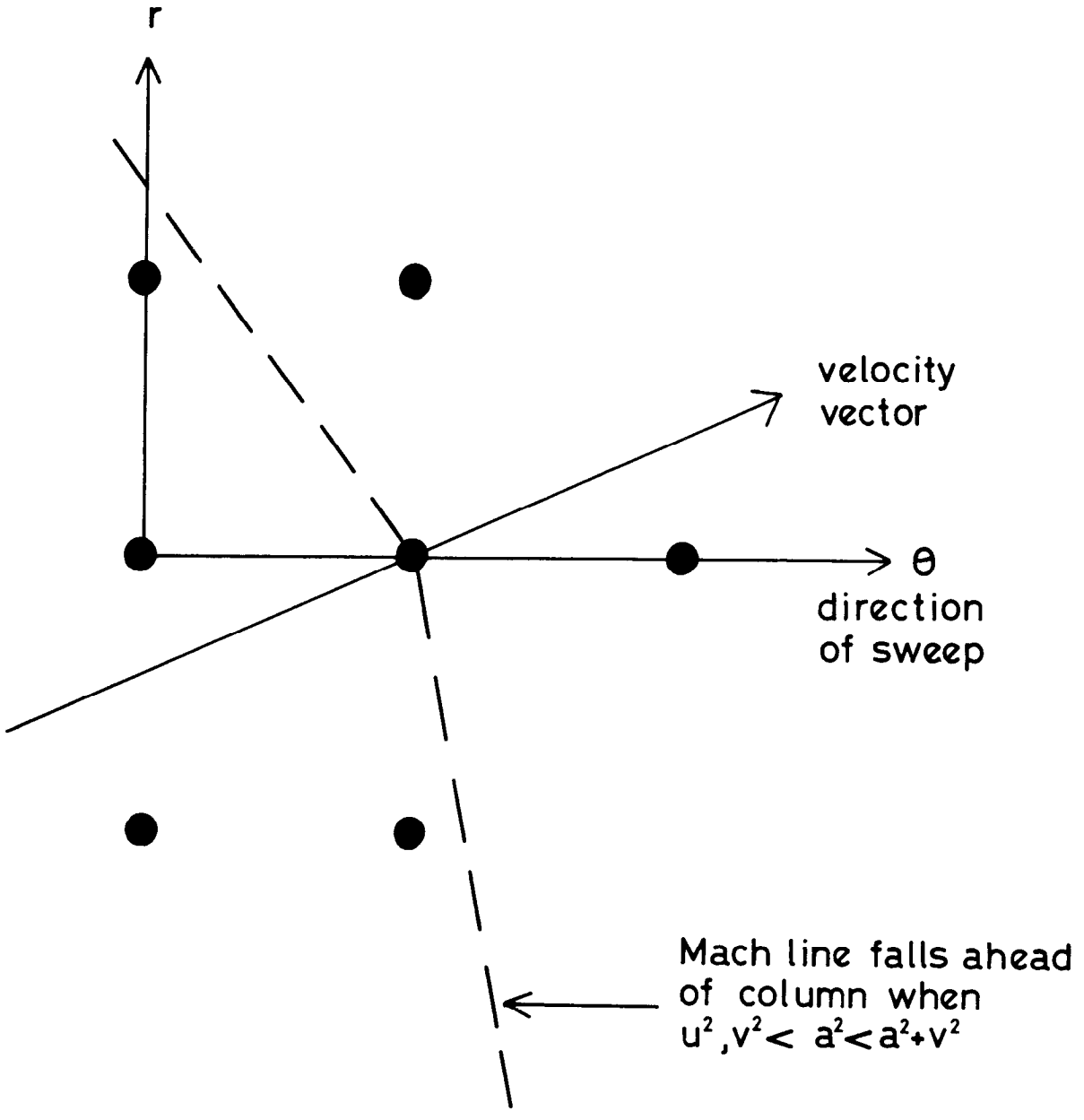

FIG. 10 IMPROPER ZONE OF DEPENDENCE FOR MURMAN IMPLICIT DIFFERENCE SCHEME

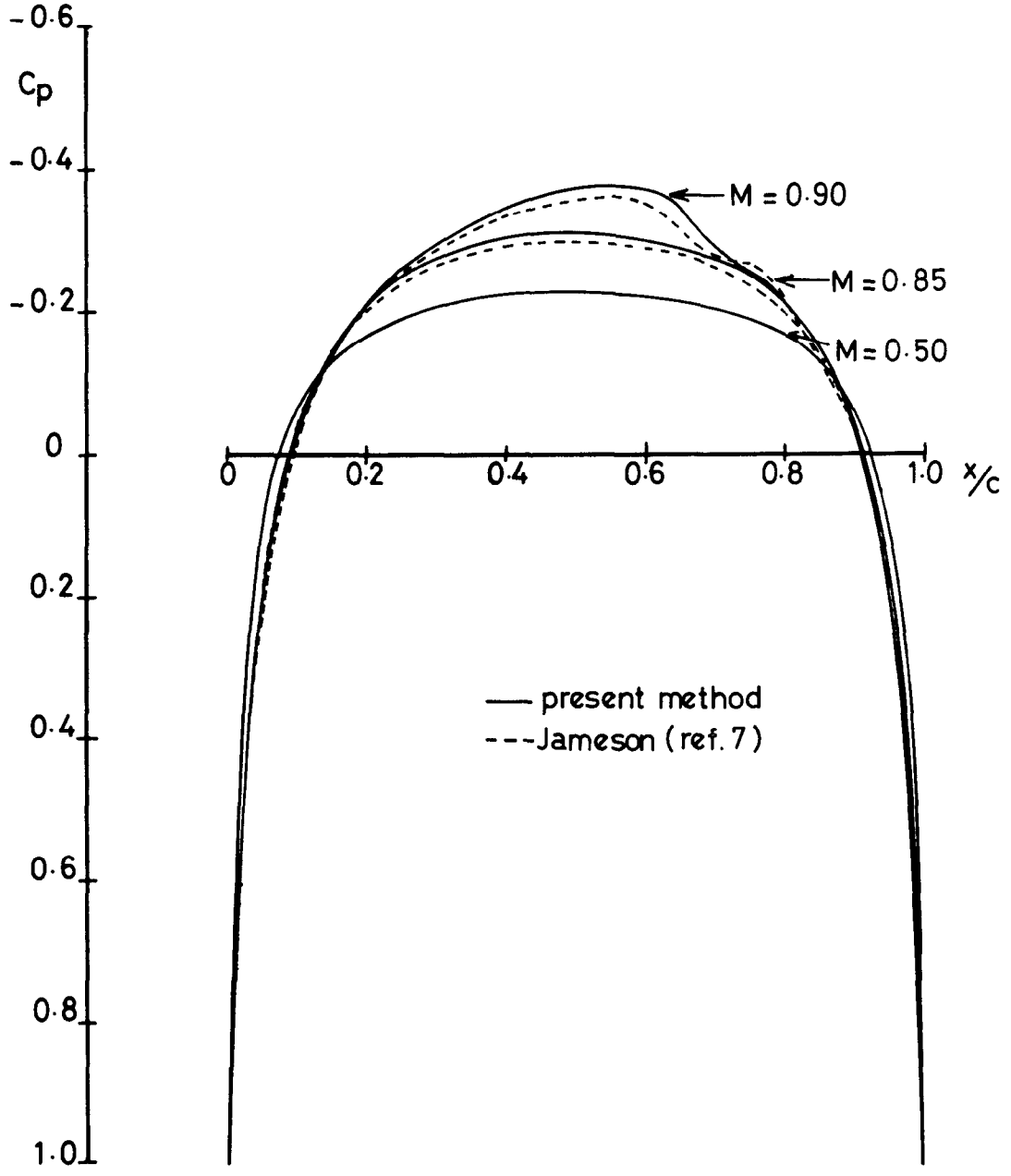

FIG. 11a CALCULATED PRESSURE DISTRIBUTIONS ON ELLIPSOID

FIG. 11b

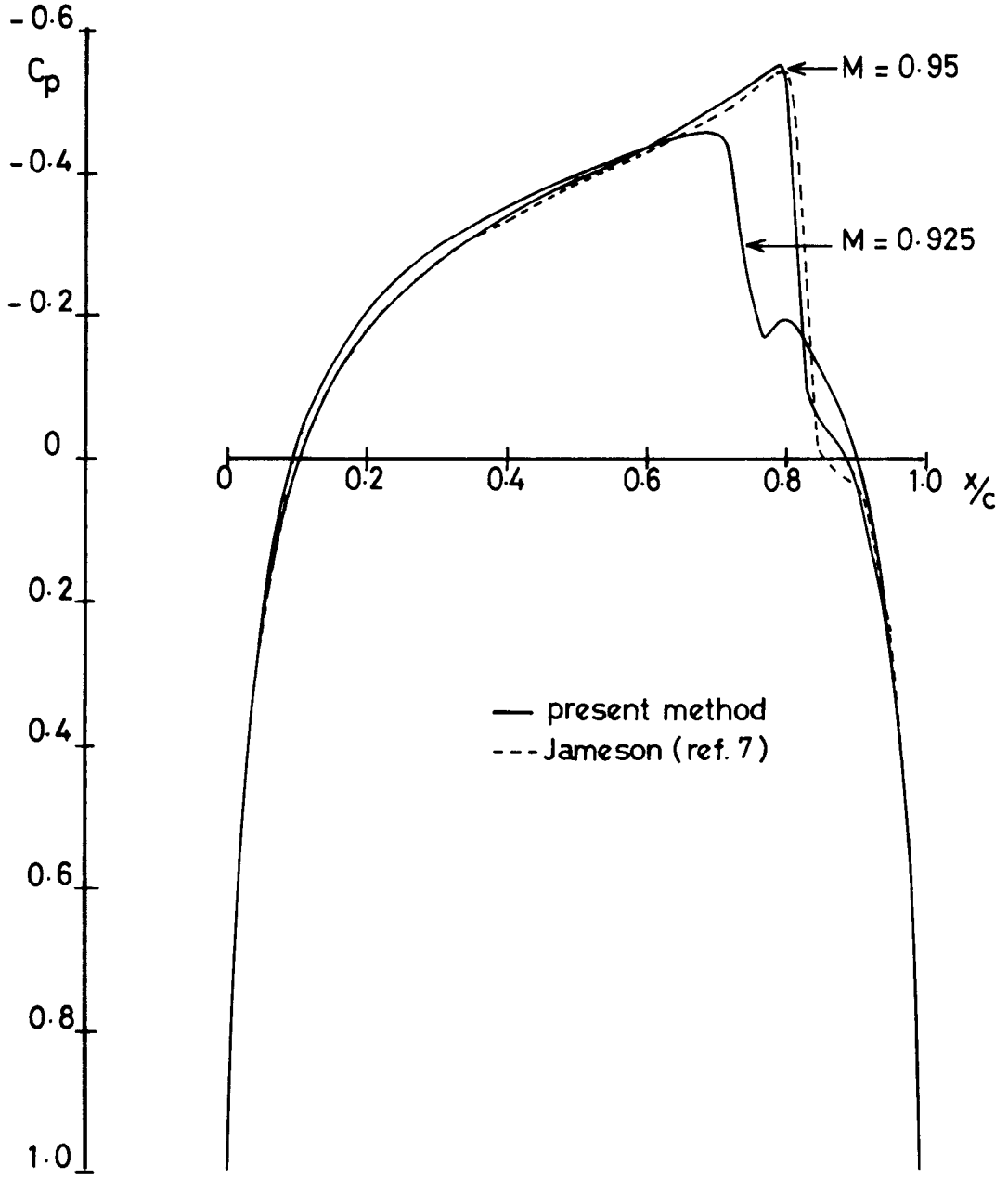

FIG. 11b CALCULATED PRESSURE DISTRIBUTIONS ON ELLIPSOID

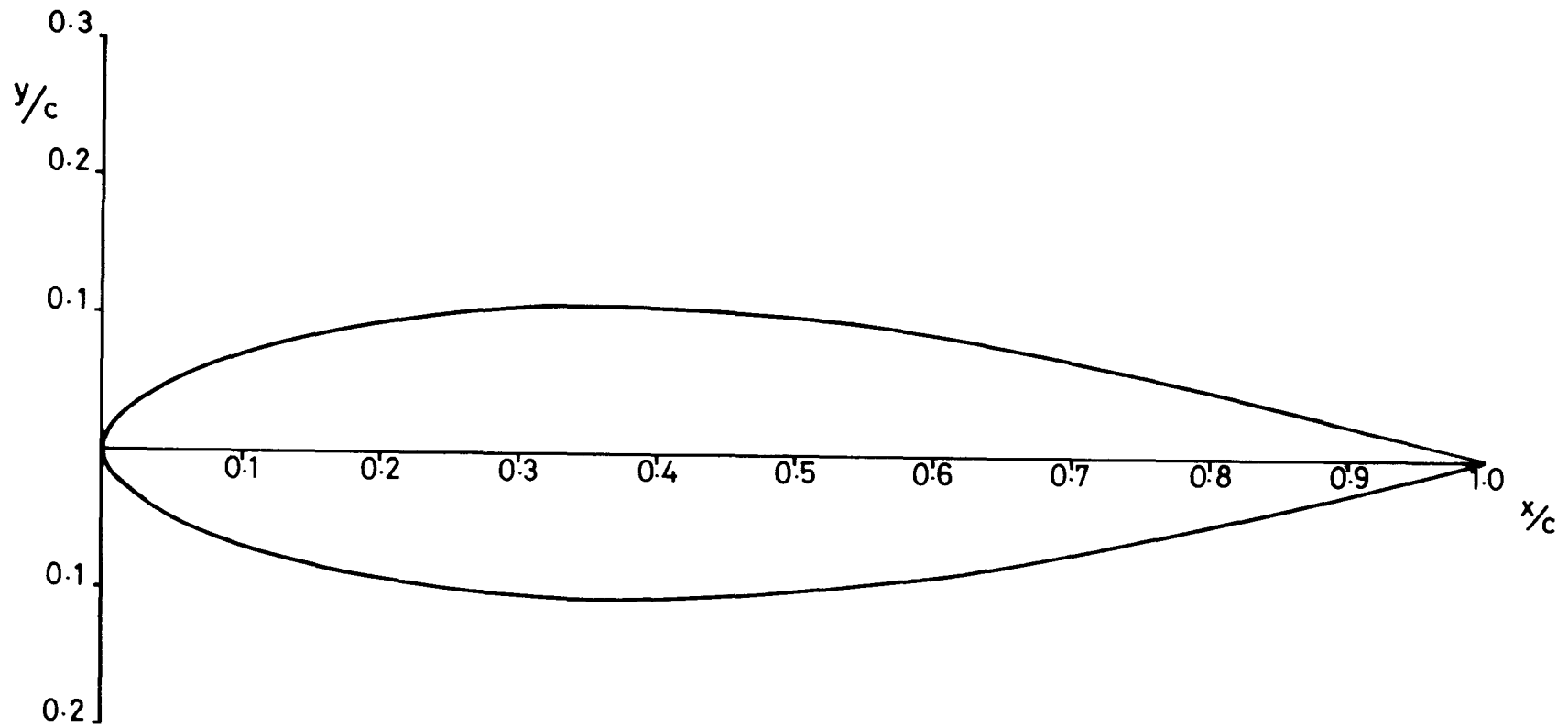

FIG. 12

BODY WITH BLUNT NOSE AND POINTED TAIL

FIG. 12

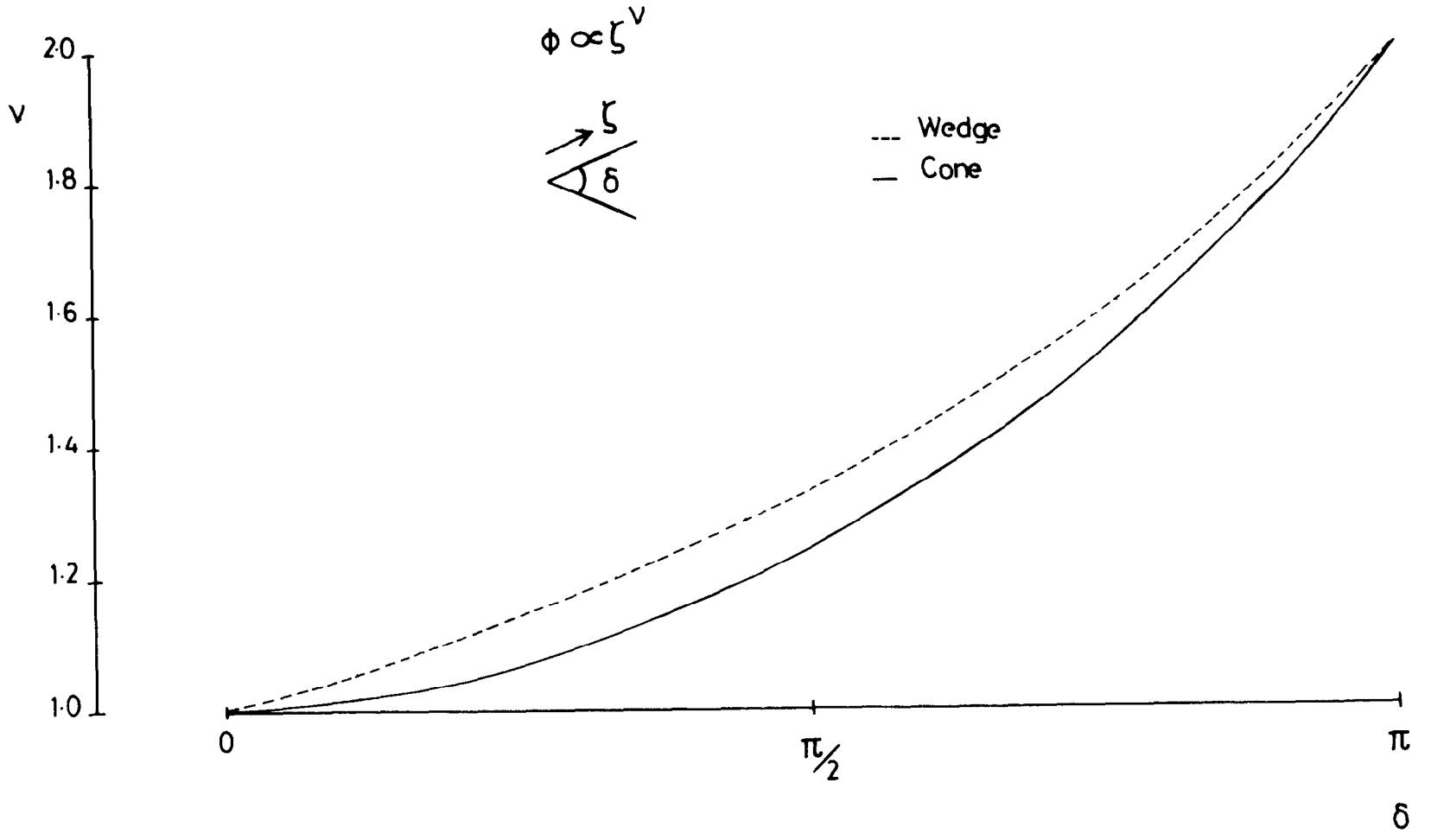

FIG. 13 BEHAVIOUR OF VELOCITY POTENTIAL NEAR TIP OF CONE & WEDGE

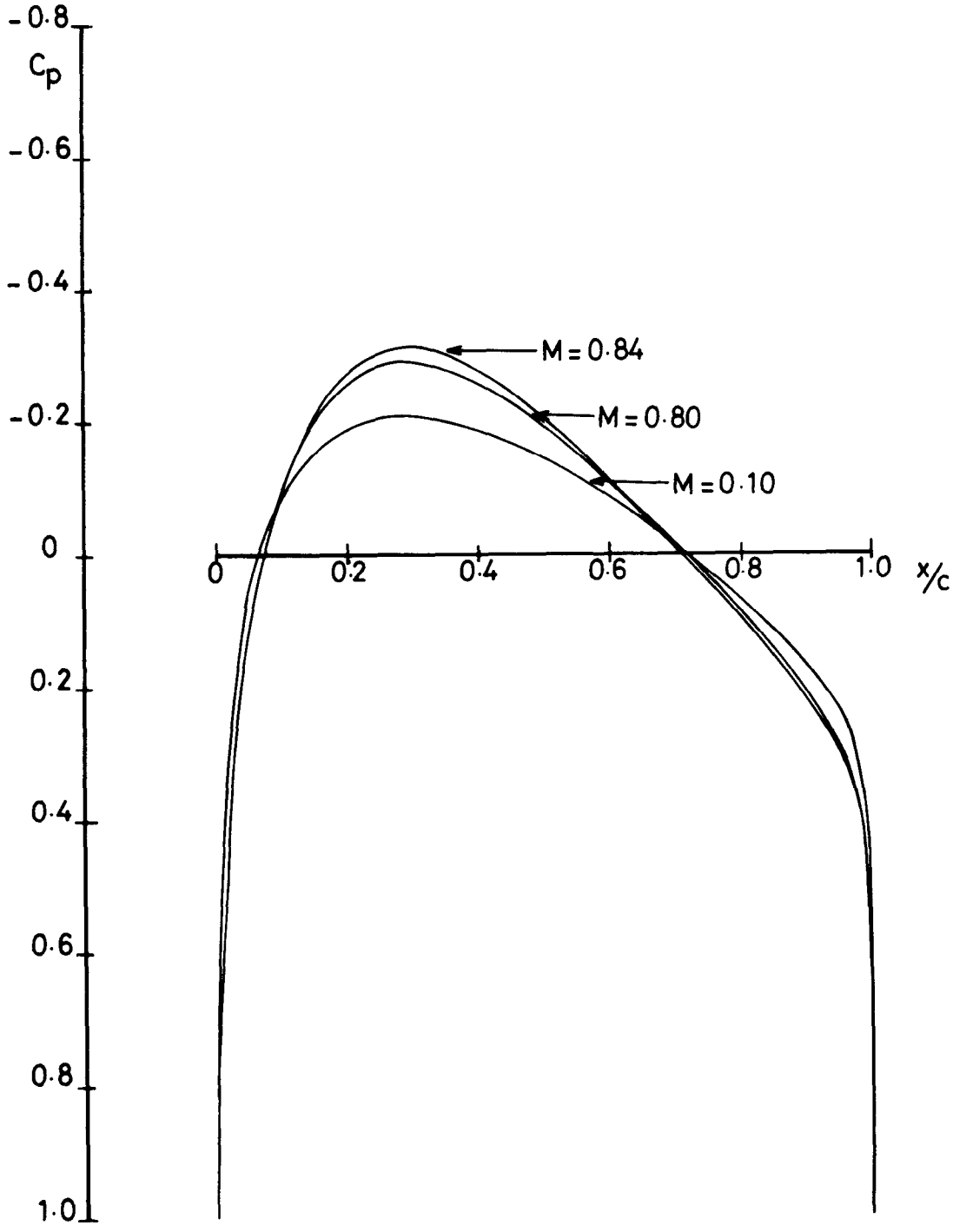

FIG. 14a CALCULATIONS ON BODY WITH BLUNT NOSE AND POINTED TAIL

FIG 14b

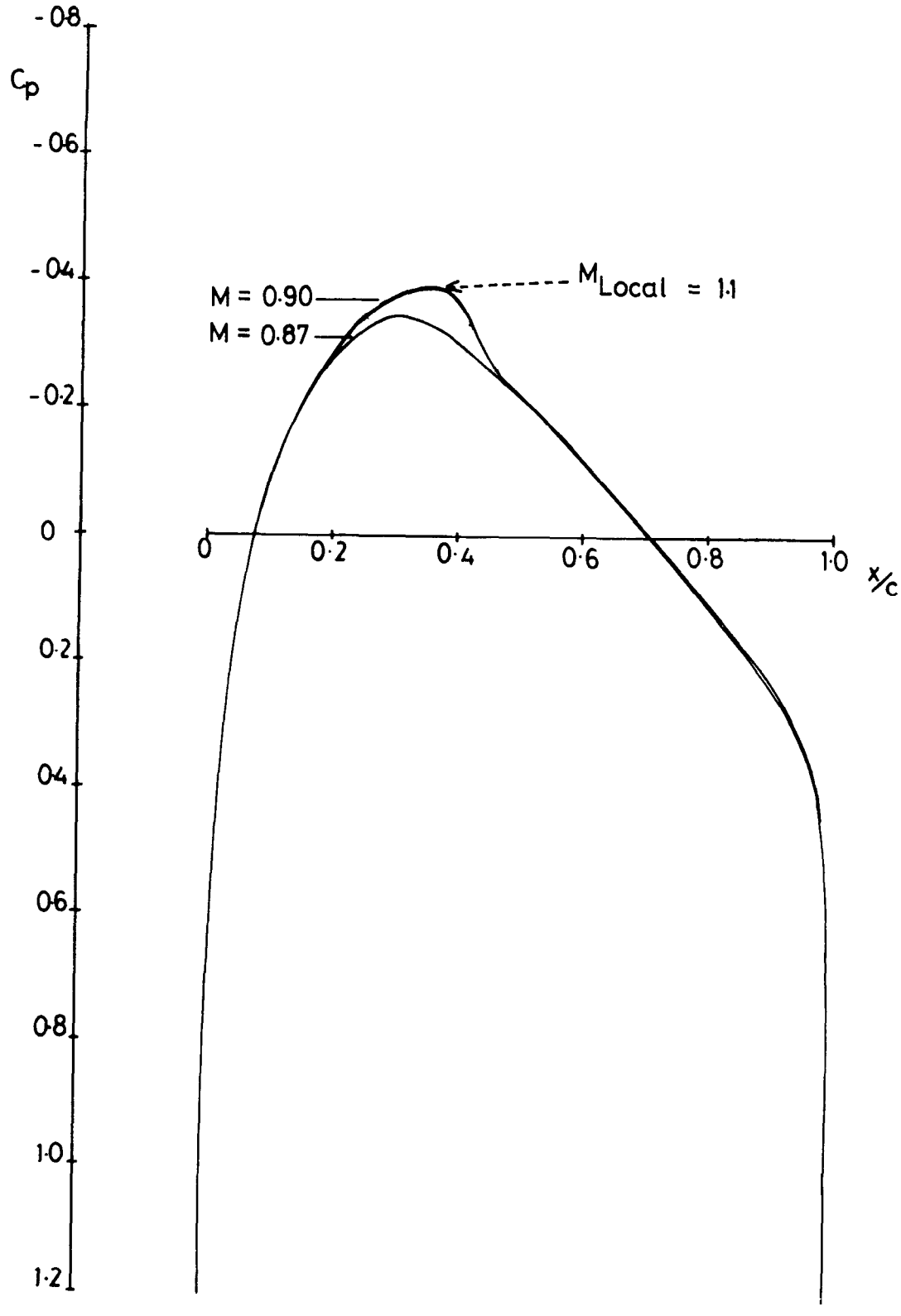

FIG. 14b CALCULATIONS ON BODY WITH BLUNT NOSE AND POINTED TAIL

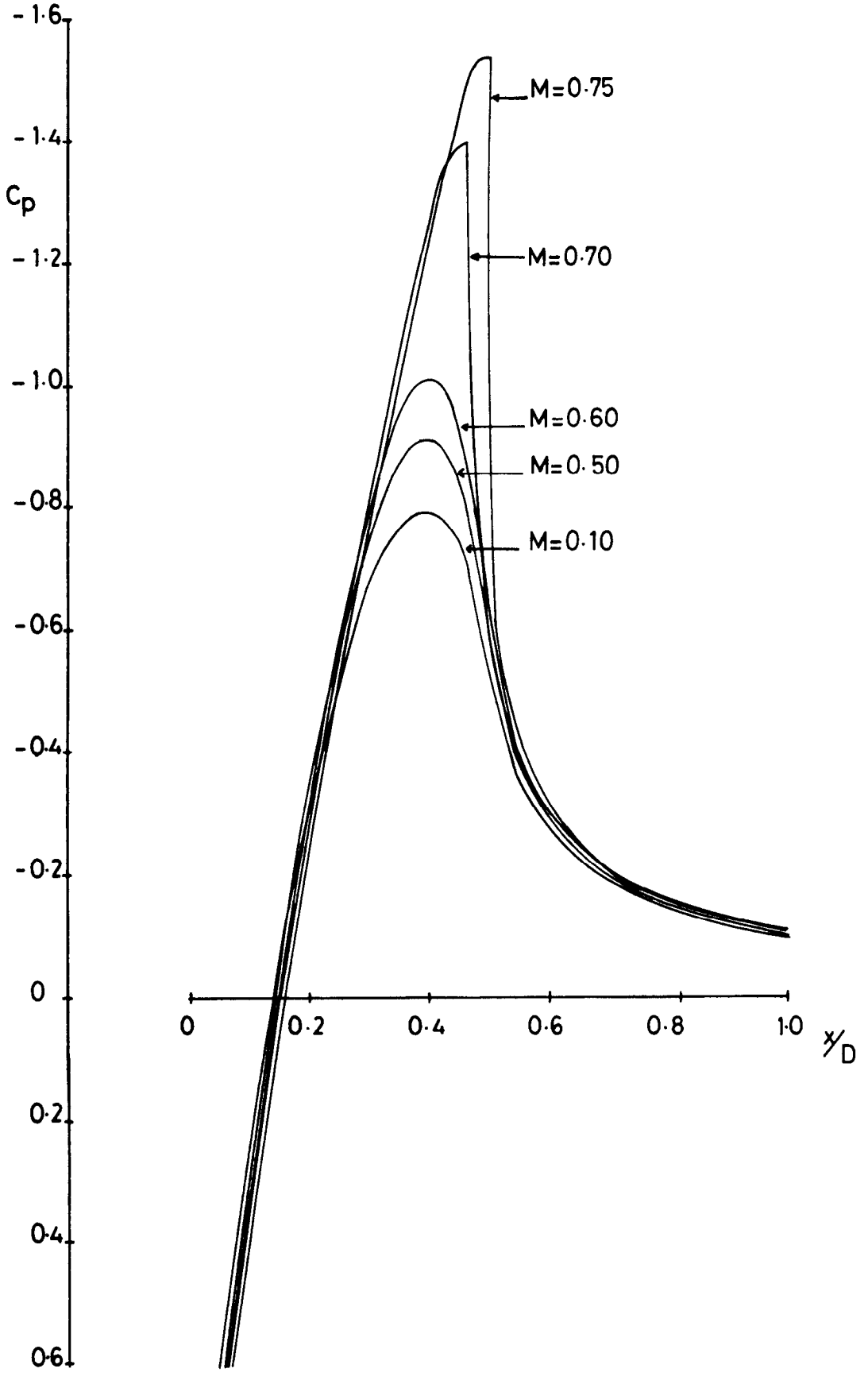

FIG. 15 CALCULATIONS FOR HEMISPHERE-CYLINDER

FIG. 16a

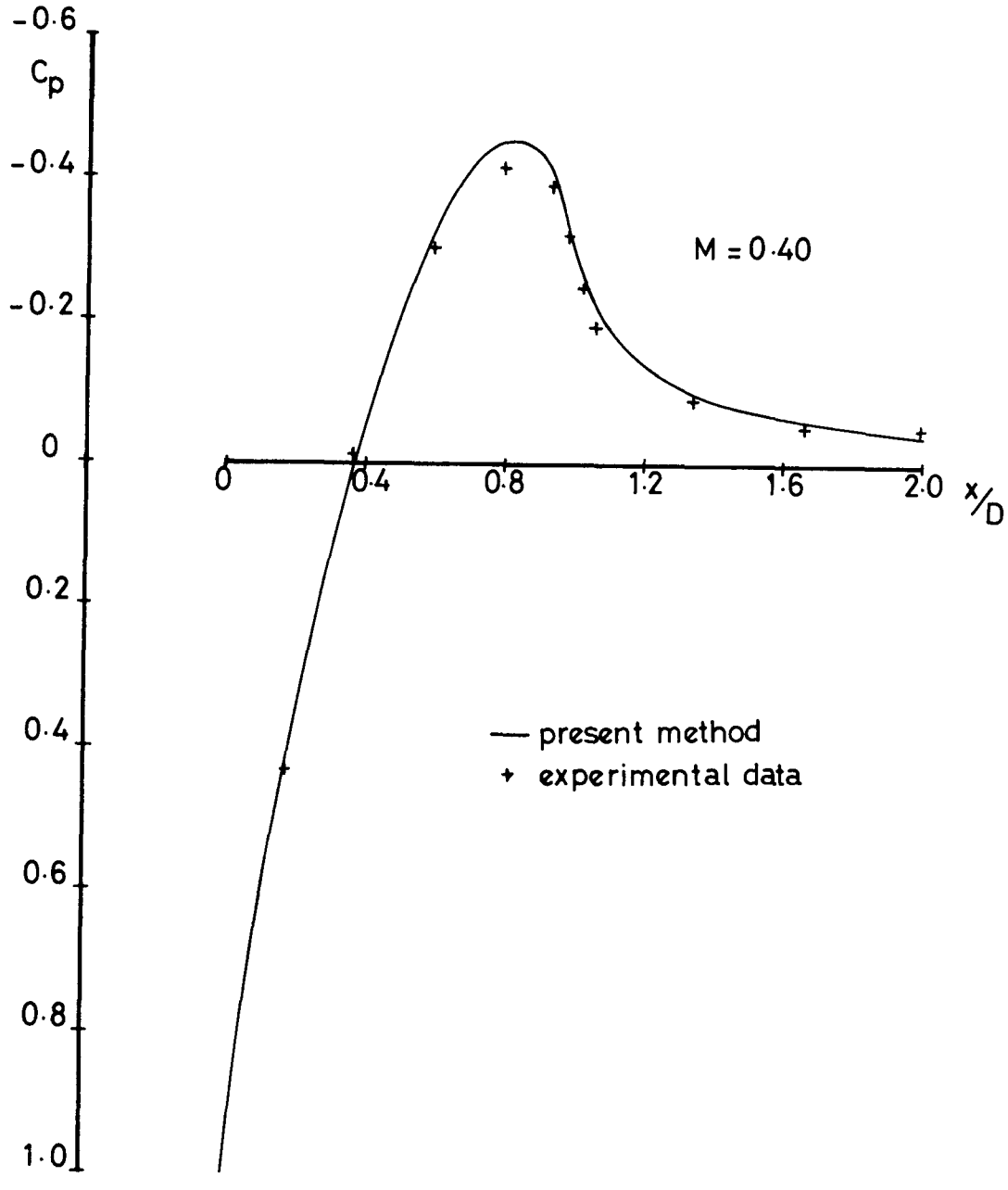

FIG. 16a CALCULATIONS FOR OGIVE - CYLINDER - COMPARISON WITH EXPERIMENTAL DATA

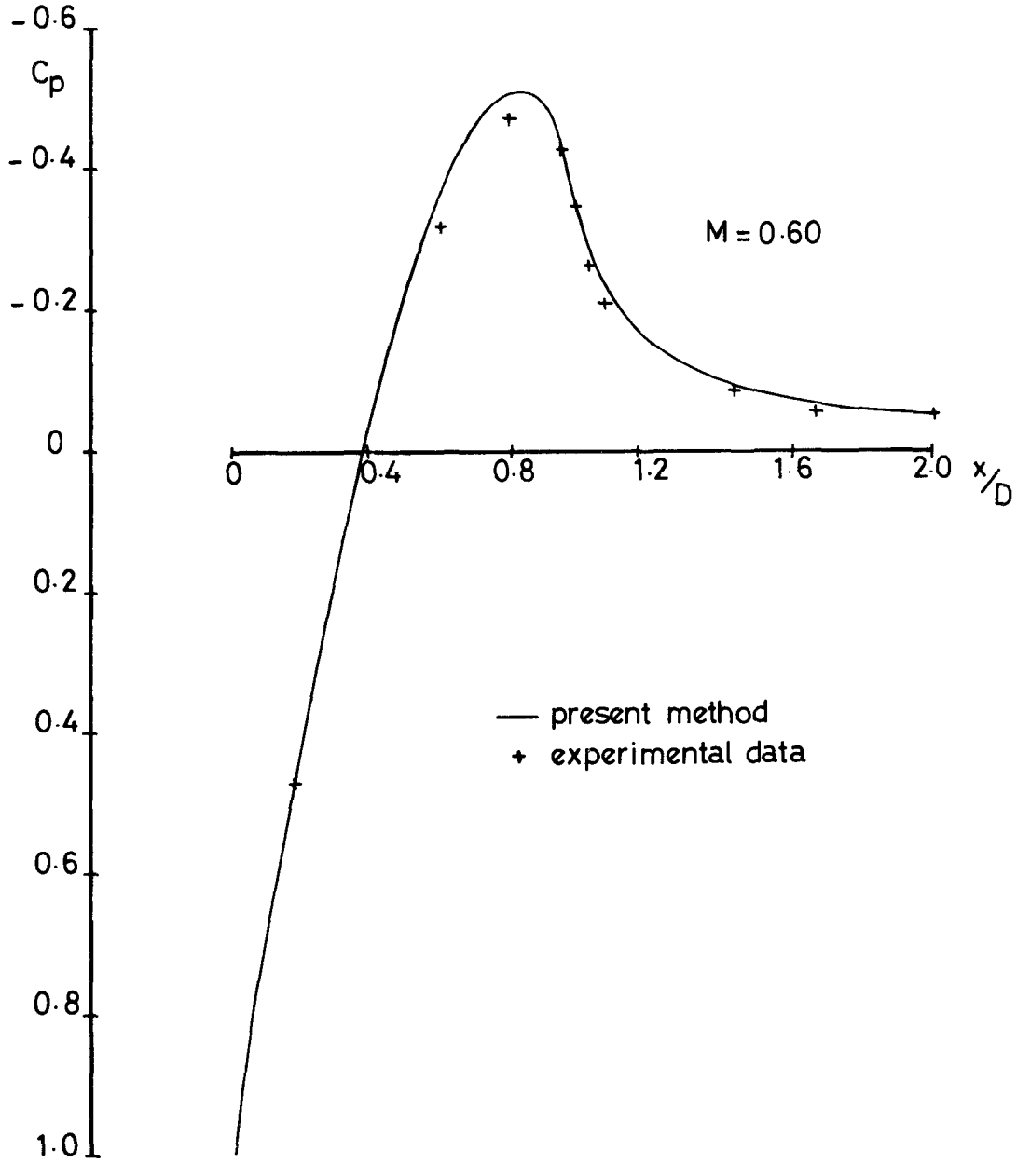

FIG. 16b CALCULATIONS FOR OGIVE - CYLINDER — COMPARISON WITH EXPERIMENTAL DATA

FIG 16c

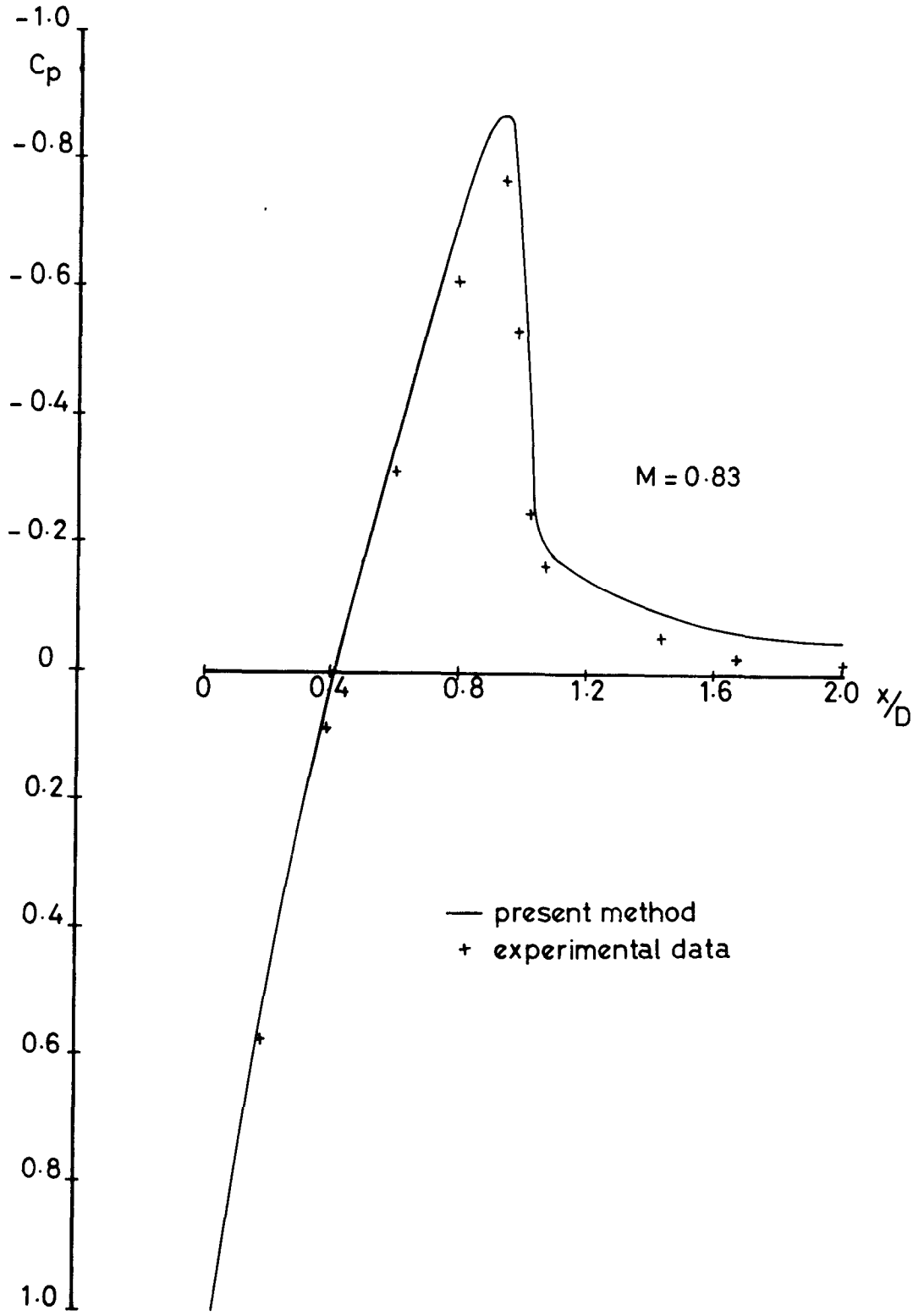

FIG. 16c CALCULATIONS FOR OGIVE - CYLINDER - COMPARISON WITH EXPERIMENTAL DATA

Produced in England by Her Majesty's Stationery Office, Reprographic Centre, Basildon
Bas 33706/Dd 587483 K5 6/77 P

ARC CP No.1376
September 1973
Langley, M.J.

NUMERICAL METHODS FOR TWO-DIMENSIONAL AND AXISYMMETRIC TRANSONIC FLOWS

Two methods are presented for the calculation of transonic flows. Firstly a method is described for the design of aerofoils with prescribed pressure distributions including shock waves. The method is essentially an inversion of a numerically refined version of the Murman-Krupp technique for the solution of the transonic small perturbation equation with linearized boundary conditions. To demonstrate the usefulness and accuracy of the method examples are shown of the design of supercritical type aerofoil

ARC CP No.1376
September 1973
Langley, M.J.

NUMERICAL METHODS FOR TWO-DIMENSIONAL AND AXISYMMETRIC TRANSONIC FLOWS

Two methods are presented for the calculation of transonic flows. Firstly a method is described for the design of aerofoils with prescribed pressure distributions including shock waves. The method is essentially an inversion of a numerically refined version of the Murman-Krupp technique for the solution of the transonic small perturbation equation with linearized boundary conditions. To demonstrate the usefulness and accuracy of the method examples are shown of the design of supercritical type aerofoil

ARC CP No.1376
September 1973
Langley, M.J.

NUMERICAL METHODS FOR TWO-DIMENSIONAL AND AXISYMMETRIC TRANSONIC FLOWS

Two methods are presented for the calculation of transonic flows. Firstly a method is described for the design of aerofoils with prescribed pressure distributions including shock waves. The method is essentially an inversion of a numerically refined version of the Murman-Krupp technique for the solution of the transonic small perturbation equation with linearized boundary conditions. To demonstrate the usefulness and accuracy of the method examples are shown of the design of supercritical type aerofoil

sections, the final results being compared with calculations by the nominally exact Garabedian & Korn analysis method.

The second method is for the calculation of axisymmetric transonic flow past bodies of revolution. Following Garabedian & Korn the exact potential flow equations are solved in the inside of the unit circle obtained from the body contour by conformal transformation. The particular problems of calculating axisymmetric flows by such methods are discussed and examples are shown of calculations by the present method compared with other methods and experimental data.

sections, the final results being compared with calculations by the nominally exact Garabedian & Korn analysis method.

The second method is for the calculation of axisymmetric transonic flow past bodies of revolution. Following Garabedian & Korn the exact potential flow equations are solved in the inside of the unit circle obtained from the body contour by conformal transformation. The particular problems of calculating axisymmetric flows by such methods are discussed and examples are shown of calculations by the present method compared with other methods and experimental data.

sections, the final results being compared with calculations by the nominally exact Garabedian & Korn analysis method.

The second method is for the calculation of axisymmetric transonic flow past bodies of revolution. Following Garabedian & Korn the exact potential flow equations are solved in the inside of the unit circle obtained from the body contour by conformal transformation. The particular problems of calculating axisymmetric flows by such methods are discussed and examples are shown of calculations by the present method compared with other methods and experimental data.

HER MAJESTY'S STATIONERY OFFICE

Government Bookshops

49 High Holborn, London WC1V 6HB
13a Castle Street, Edinburgh EH2 3AR
41 The Hayes, Cardiff CF1 1JW
Brazennose Street, Manchester M60 8AS
Southey House, Wine Street, Bristol BS1 2BQ
258 Broad Street, Birmingham B1 2HE
80 Chichester Street, Belfast BT1 4JY

Government publications are also available through booksellers

C.P. No. 1376

ISBN 0 11 471122 4